Spin wave instability processes in ferrites

Ming Chen and Carl E. Patton
Department of Physics
Colorado State University
Fort Collis, Colorado

Chapter 3
pages 33 - 82

Nonlinear Phenomena and Chaos in Magnetic Materials

P. E. Wigen, editor
World Scientific Publishing Company, Ltd.,
Singapore, 1994.

Table of Contents

1. Introduction 1

2. Classical Formalism 3
2.1. Magnetic Torque Equation 3
2.2. Effective Fields 7
2.3. Equation of Motion 11

3. Linear Response Theory 13
3.1. Uniform Mode and Ferromagnetic Resonance 13
3.2. Spin Wave Dispersion 15

4. Spin Wave Instability Processes 19
4.1. Spin Wave Equation of Motion 19
4.2. First Order Spin Wave Instability 21

5. Parallel Pumping Instability 24
5.1. Parallel Pumping Instability Threshold 25
5.2. Spin Wave Linewidth Effect 28

6. Subsidiary Absorption 31
6.1. Perpendicular Pumping Instability Threshold 31
6.2. Spin Wave Linewidth Effect 37

7. Conclusion 41

Appendix A. Magnetostatic Approximation 43
Appendix B. Holstein-Primakoff Transformation 45
References 50

CHAPTER 3

SPIN WAVE INSTABILITY PROCESSES IN FERRITES

Ming Chen and Carl E. Patton
Department of Physics, Colorado State University
Fort Collins, CO 80523, USA

1. Introduction

Magnetic excitations in ferrites at microwave frequencies have been a subject of continuing study since the discovery of ferromagnetic resonance (FMR) by Griffiths [1]. A typical FMR experiment involves a ferromagnetic or ferrimagnetic sample subjected to a static magnetic field and a microwave magnetic field in a perpendicular configuration. By sweeping the static field in magnitude over a certain range and monitoring the microwave power absorbed by the sample, an absorption peak is observed. It is found that, at low microwave power levels, the absorbed power by the sample is proportional to the pumping power, and the field position of the resonance peak changes with the pump microwave frequency and the shape of the sample. This phenomenon was first explained by Kittel [2,3] in his linear response theory for FMR as the resonance absorption of microwave power by the "uniform mode," or the in-phase Larmor precessional motion of the magnetization vector in the sample.

As the level of the microwave power is increased, however, magnetic excitations with nonlinear behavior have been observed over a broad range of the static field. High power effects in ferrite materials were first observed by Bloembergen, Damon, and Wang in FMR experiments [4-7]. A typical set of data is shown in Fig. 1-1. In the figure, the solid curve with open triangles is the FMR response at low power and the curve with open circles is the response at high power. At high microwave power levels, two new effects are found. One is the broad "subsidiary absorption" region at static fields somewhat lower than those for the FMR peak. The other is the broadening of the narrow FMR peak. This broadening occurs at microwave power levels much lower than expected from classical FMR theory and is often called "premature saturation." These nonlinear effects are associated with a pump field applied perpendicular to the static field. When a microwave field is applied parallel to the static field direction, a nonlinear effect also occurs at high power levels in the form of a broad absorption region like subsidiary absorption, but at even lower static fields. This effect is usually called "parallel pumping instability."

These initial observations have led to a detailed ongoing study of the nonlinear microwave properties of ferrites, nonlinear spin wave interactions, and spin wave

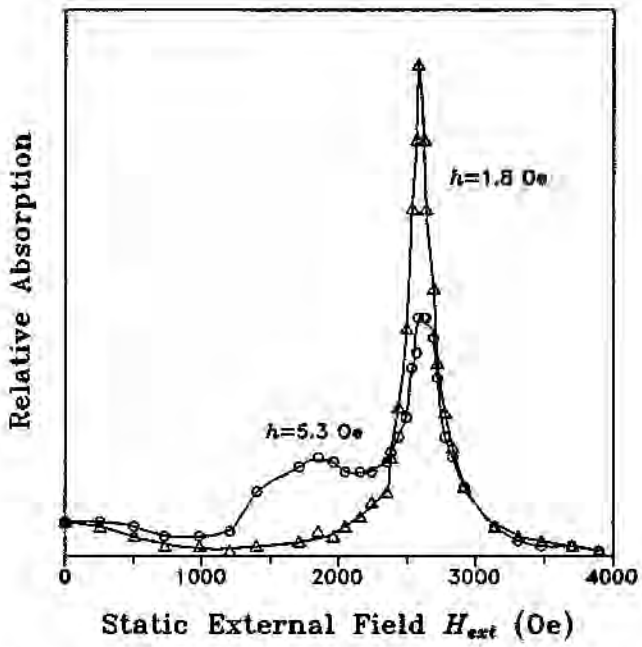

Figure 1-1 Ferromagnetic resonance absorption curves at low power (triangles) and high power (circles) for a [111] magnetized single crystal nickel ferrite sphere at 9.4 GHz [7].

relaxation processes. The spin wave instability theory developed by Suhl [8] and Schlömann [9] has been successful in accounting for these microwave processes in ferrites at high power levels. According to the theory, the parametric excitation of spin waves leads to various instabilities. These instability effects are the result of two competing processes, damping due to spin wave relaxation loss and growth due to the microwave pumping. At low power levels, the power coupled into the spin waves is small and the spin wave amplitudes stay at thermal equilibrium values. Within this regime, the response to the pump microwave field is linear. The nonlinear effects occur at some critical power level above which certain spin waves are parametrically excited by the microwave pumping.

This chapter provides a review of the basic aspects of spin wave instability processes. The chapter starts with a general classical formalism for magnetic systems derived from the magnetic torque equation and the Maxwell equations. We examine the linear response theory for ferromagnetic resonance and spin waves. We then discuss the spin wave instability theory by extending the linear spin wave theory to include the first order nonlinear contributions. Finally, we compare the theoretical results with experimental data on the parallel pumping and the subsidiary absorption effects. The focus is on first order processes, following the terminology of Schlömann [9]. Second order instability processes and other nonlinear effects, such as the steady state response above threshold, auto-oscillation and chaos, are not considered in this chapter.

2. Classical Formalism

The concept of spin waves was first introduced by Bloch [10], on a quantum-mechanical basis, to describe the progressive variation of phase and amplitude of spin dipole precession in ferromagnetic materials. This concept was later adopted by Herring and Kittel [11] in a classical manner to describe the continuous phase variation of the precessional motion of a macroscopic magnetization vector. The spin wave model has been widely used to investigate fundamental processes of energy loss in ferromagnetic materials, and the importance of spin wave theory in microwave and millimeter wave device applications has been clearly demonstrated.

Macroscopic spin wave theory is based on a classical model of the spin system in which spin waves are treated as spatial disturbances of continuous magnetization rather than discrete spin moments in the lattice. Like any other electromagnetic wave problem, the behaviors of various spin waves can be studied by expanding the magnetization vector in a spatial Fourier series. The spin wave wavenumber is assumed to be much larger than both the wavenumber of light at the same frequency and the reciprocal of the sample dimension. In this limit, one can neglect electromagnetic propagation effects and sample shape effects.

2.1. Magnetic Torque Equation

The magnetic moment equation of motion was first proposed by Landau and Lifshitz [12], based on a magnetic torque model. This torque equation was first applied to microwave magnetics by Kittel [2,3] in his theory for ferromagnetic resonance. The equation of motion of a magnetization vector **M** may be written

$$\frac{d\mathbf{M}}{dt} = -|\gamma|\,\mathbf{M}\times\mathbf{H}_{\text{eff}}\,, \tag{2-1}$$

where $|\gamma|$ is the absolute value of the gyromagnetic ratio and $\mathbf{H}_{\text{eff}}$ is the total effective magnetic field acting on the magnetization vector. In general, **M** and $\mathbf{H}_{\text{eff}}$ must be considered as functions of space and time. The value of $|\gamma|$ for electron spins is 1.76×10^{7} rad/(s·Oe), or $2\pi\times2.80$ MHz/Oe, in Gaussian units. Many works write the right-hand side of Eq. (2-1) as $\gamma\mathbf{M}\times\mathbf{H}_{\text{eff}}$ and take γ as negative for electron spins. Other works write the same equation and use positive γ. We will use the form in Eq. (2-1) to avoid confusion.

Equation (2-1) describes the precessional motion of a magnetization vector **M** around an effective field $\mathbf{H}_{\text{eff}}$. This is most easily visualized for an infinite medium with a uniform magnetization and a uniform static internal field $\mathbf{H}_{\text{int}}$. This basic response is shown in Fig. 2-1. The vector **M** precesses around $\mathbf{H}_{\text{int}}$ as shown. This precession sense is usually termed Larmor precession. Precession in the opposite sense is termed anti-Larmor precession.

The magnetic torque equation also demands that the amplitude of the magnetization $|\mathbf{M}|$ be a constant of the motion. We write this condition as

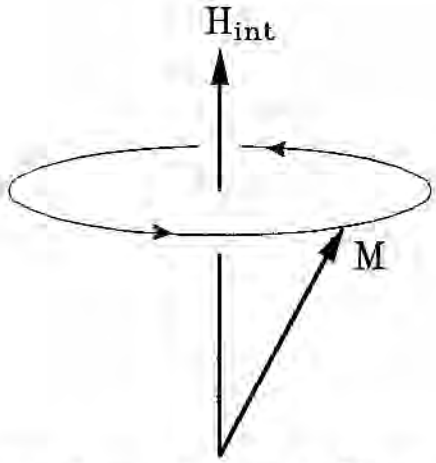

Figure 2-1 The precessional motion of a magnetization vector **M** around an internal magnetic field $\mathbf{H}_{int}$.

$$|\mathbf{M}| = M_s \ , \tag{2-2}$$

where the constant M_s denotes the saturation magnetization. Note that in formal analyses based on Gaussian units, the saturation magnetic induction $4\pi M_s$ appears more often than the saturation magnetization M_s. For typical yttrium-iron-garnet (YIG) material, the value of $4\pi M_s$ is 1750 Gauss and the value of M_s is 139.3 emu/cm^3. This work utilizes the Gaussian unit system. This is the most used system of units in the past and current literature for magnetics.

Consider an isotropic ferromagnetic insulator of ellipsoidal shape, magnetized to saturation in the z-direction by some static external magnetic field $\mathbf{H}_{ext}$. The total magnetization vector **M** is taken to have a large static component $M_s\ \mathbf{e}_z$ and a small dynamic component $\mathbf{m}(\mathbf{r},t)$.

$$\mathbf{M}(\mathbf{r},t) = M_s \mathbf{e}_z + \mathbf{m}(\mathbf{r},t) \ . \tag{2-3}$$

Here $\mathbf{e}_z$ is the unit vector parallel to the z-axis. We assume the dynamic magnetization to be of small amplitude, such that $|\mathbf{m}(\mathbf{r},t)| \ll M_s$ is satisfied. Typically, we will use upper case symbols to represent static quantities and lower case to represent dynamic quantities.

In order to analyze the dynamic magnetic response, $\mathbf{m}(\mathbf{r},t)$ is expanded in a spatial Fourier series

$$\mathbf{m}(\mathbf{r},t) = \mathbf{m}_0(t) + \sum_{k\neq 0} \mathbf{m}_k(t)\ e^{-i\mathbf{k}\cdot\mathbf{r}} \ . \tag{2-4}$$

Here $\mathbf{m}_0(t)$ denotes the uniform part of the dynamic magnetization and is usually referred to as the "uniform mode." The Fourier components $\mathbf{m}_k(t)$ with $k\neq 0$ define the nonuniform part of the dynamic magnetization. Note that when the wavevector **k** occurs as a subscript or summation index, the vector notation will be omitted for simplicity.

Also note that the $\mathbf{m}_k(t)$ terms in Eq. (2-4) are complex, while the total $\mathbf{m}(\mathbf{r},t)$ and the uniform mode $\mathbf{m}_0(t)$ terms are real. The total response for $k\neq 0$ part of $\mathbf{m}(\mathbf{r},t)$ is made real by the sum over $\pm\mathbf{k}$ terms in the overall expansion. The relation between $\mathbf{m}_k(t)$ and $\mathbf{m}_{-k}(t)$ is given by

$$\mathbf{m}_k^*(t) = \mathbf{m}_{-k}(t) \quad . \tag{2-5}$$

This connection will play an important role in the spin wave instability theory developed in Sec. 4.

The $\mathbf{m}_0(t)$ uniform mode term describes the in-phase and spatially uniform component of the dynamic response. At low microwave power levels, this is often the main mode excited by a uniform microwave pump field. Diagram (a) in Fig. 2-2 depicts the uniform mode discussed above. Here, all the magnetization vectors are precessing uniformly in phase about the direction of the external field.

The $\mathbf{m}_k(t)\exp(-i\mathbf{k}\cdot\mathbf{r})$ terms in the expansion, in contrast, describe the propagating, time dependent components of the dynamic magnetization. These terms constitute classical spin waves. The $\mathbf{m}_k(t)$ are taken to vary as $\exp(\pm i\omega_k t)$. The phase factors of the classical spin waves are of the form $\exp[-i(\mathbf{k}\cdot\mathbf{r}\pm\omega_k t)]$, as for other electromagnetic plane waves.

To visualize the way spin waves propagate, schematic views of the motions of different spin moments are given in diagrams (b) and (c) of Fig. 2-2. Diagrams (b) and (c) show spin waves in schematic form for two key propagation directions, parallel or perpendicular to the static internal field, respectively. For $\mathbf{k}$ parallel to the static field, the divergence of the magnetization, $\nabla\cdot\mathbf{m}$, is zero. For $\mathbf{k}$ perpendicular to the field, the magnetization has a nonzero divergence and dipole fields are generated. These fields may be viewed as arising from magnetic charges ρ_m which derive from $\rho_m=-4\pi\nabla\cdot\mathbf{m}$. The dipole field, generated by the nonzero $\nabla\cdot\mathbf{m}$ when $\mathbf{k}$ and $\mathbf{H}_{ext}$ are not parallel, has two effects: (1) The fields tend to raise the energy of the spin-system. (2) The fields alter the spin motion from a circular precession to an elliptical precession cone. These effects will be manifest in the treatments to follow.

We introduce a Cartesian coordinate system (x,y,z) as shown in Fig. 2-3. The z-axis of the system is chosen to be parallel to the static internal field $\mathbf{H}_{int}$ vector. The static saturation magnetization $\mathbf{M}_s$ is also along z-direction. For a spin wave with wavevector $\mathbf{k}$ in an arbitrary direction, the x-, y-, and z-components of the wavevector are (k_x,k_y,k_z). These components may be expressed in terms of the wave number k, the polar angle θ_k, and the azimuthal angle ϕ_k, also shown in Fig. 2-3.

Even though we write $\mathbf{m}(\mathbf{r},t)$ as a general three-component vector, only $m_x(\mathbf{r},t)$ and $m_y(\mathbf{r},t)$ are independent amplitude components. The condition $|\mathbf{M}|=M_s$ yields a z-component which is second order in the x- and y-components.

$$m_z(\mathbf{r},t) \approx -\frac{1}{2M_s}[m_x^2(\mathbf{r},t)+m_y^2(\mathbf{r},t)] \quad . \tag{2-6}$$

In the linear theory, this m_z term is usually ignored. In the nonlinear theory, however,

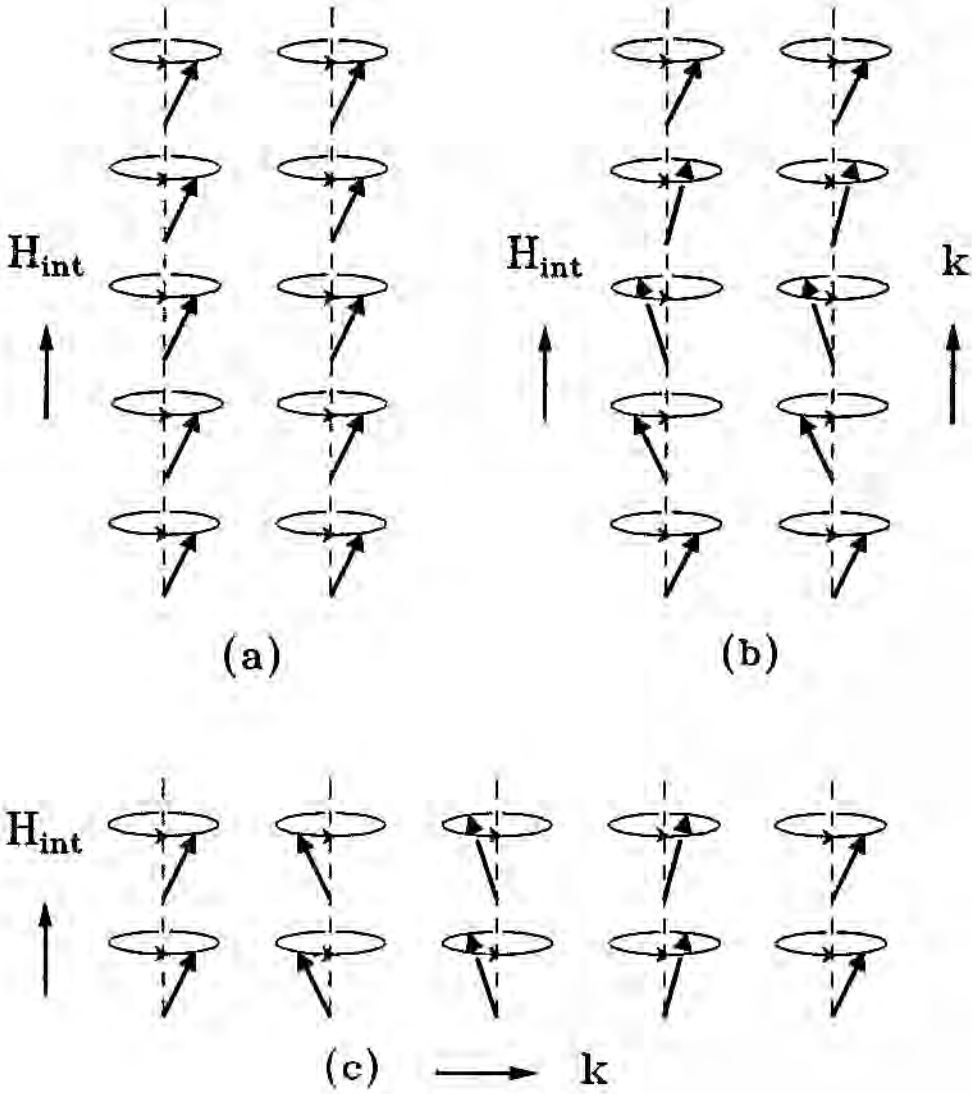

Figure 2-2 Schematic illustrations of (a) the uniform mode and spin waves with wavevector **k** (b) parallel to, and (c) perpendicular to the static internal field $\mathbf{H}_{int}$.

the second order m_x and m_y terms which appear in m_z play an important role. The Fourier components for the uniform mode, $m_{0z}(t)$, and spin waves, $m_{kz}(t)$, can be shown to have leading terms in second order as given below.

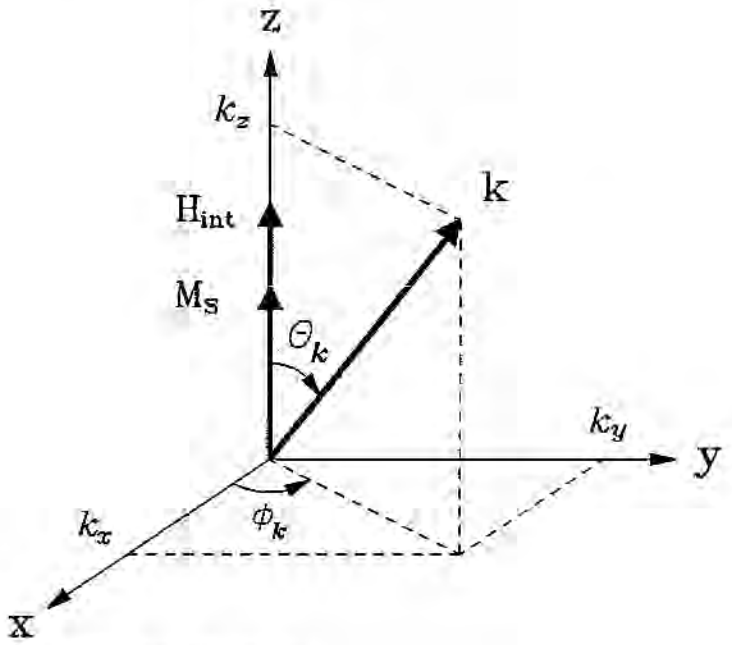

Figure 2-3 Coordinate system for spin waves.

$$m_{0z}(t) \approx -\frac{1}{2M_s}[m_{0x}^2(t) + m_{0y}^2(t)] \ . \tag{2-7a}$$

$$m_{kz}(t) \approx -\frac{1}{M_s}[m_{0x}(t)\, m_{kx}(t) + m_{0y}(t)\, m_{ky}(t)] \ . \tag{2-7b}$$

Such terms involving $m_{0z}(t)$ and $m_{kz}(t)$ may enter into the x- and y-component equations through various terms in the effective field $\mathbf{H}_{eff}$, as will be considered shortly.

2.2. *Effective Fields*

The total effective field $\mathbf{H}_{eff}(\mathbf{r},t)$ in the magnetic torque equation for an isotropic ferromagnetic medium consists of five fields: an applied static external field $\mathbf{H}_{ext}$, the static demagnetizing field $\mathbf{H}_{dem}$, an applied microwave pump field $\mathbf{h}_p(t)$, the dipole field $\mathbf{h}_{dip}(\mathbf{r},t)$, and the effective exchange field $\mathbf{h}_{ex}(\mathbf{r},t)$.

$$\mathbf{H}_{eff}(\mathbf{r},t) = \mathbf{H}_{ext} + \mathbf{H}_{dem} + \mathbf{h}_p(t) + \mathbf{h}_{dip}(t) + \mathbf{h}_{ex}(\mathbf{r},t) \ . \tag{2-8}$$

For simplicity, the contribution of anisotropy is not included.

The first field in $\mathbf{H}_{eff}(\mathbf{r},t)$ is the applied static external field $\mathbf{H}_{ext}$. This $\mathbf{H}_{ext}$ is taken to be sufficient to magnetize the sample to saturation along the z-direction. The second field in $\mathbf{H}_{eff}(\mathbf{r},t)$ is the demagnetizing field $\mathbf{H}_{dem}$. The demagnetizing field is the static dipole field generated by the static magnetization $\mathbf{M}_s$ for a finite size sample and

generally related to the shape of the sample. For $\mathbf{M}_s$ along $\mathbf{e}_z$, this field is given by

$$\mathbf{H}_{dem} = -4\pi M_s \mathbf{N} \cdot \mathbf{e}_z \tag{2-9a}$$

where $\mathbf{N}$ is a 3×3 demagnetizing factor tensor for a sample with ellipsoidal shape. When the three principal axes of the ellipsoidal sample coincide with the x-, y-, and z-axes, only the diagonal elements in the tensor are nonzero and denoted as N_x, N_y, and N_z. For $\mathbf{H}_{ext}$ and $\mathbf{M}_s$ in the z-direction, the demagnetizing field is simply

$$\mathbf{H}_{dem} = -4\pi M_s N_z \mathbf{e}_z \ . \tag{2-9b}$$

We combine $\mathbf{H}_{ext}$ and $\mathbf{H}_{dem}$ to form the static internal field $\mathbf{H}_{int}$.

$$\mathbf{H}_{int} = (H_{ext} - 4\pi M_s N_z)\ \mathbf{e}_z \ . \tag{2-10}$$

Note that for spheres, we have $N_x=N_y=N_z=1/3$. For samples of other shapes, $\mathbf{H}_{ext}$ may not always be parallel to $\mathbf{H}_{int}$. Static equilibrium always requires that $\mathbf{M}_s$ be aligned along $\mathbf{H}_{int}$. The analyses in this chapter are limited mostly to spherical samples.

The third field in $\mathbf{H}_{eff}(\mathbf{r},t)$ is the applied microwave pump field $\mathbf{h}_p(t)$. The microwave pump field is used as an excitation field for the spin system in the sample. It may be applied parallel to the static internal field ("parallel pumping"), perpendicular to the static internal field ("perpendicular pumping"), or at an arbitrary angle ("oblique pumping"). In this chapter, we will concentrate on the parallel pumping and the perpendicular pumping situations.

The fourth field in $\mathbf{H}_{eff}(\mathbf{r},t)$ is the dipole field $\mathbf{h}_{dip}(\mathbf{r},t)$. The dipole field is the dynamic magnetic field in the sample due to the dipole-dipole interaction of the precessing magnetic moments in the spin system. This includes the effects of both the uniform precession and the spin wave components of the dynamic magnetization $\mathbf{m}(\mathbf{r},t)$. The dipole field is taken to satisfy Maxwell equations in the form

$$\nabla \times \mathbf{h}_{dip}(\mathbf{r},t) = 0 \tag{2-11}$$

and

$$\nabla \cdot [\mathbf{h}_{dip}(\mathbf{r},t) + 4\pi \mathbf{m}(\mathbf{r},t)] = 0 \ . \tag{2-12}$$

Equation (2-11) is obtained from Maxwell equations under the so-called "magnetostatic approximation," which assumes that the spatial variations of $\mathbf{h}_{dip}(\mathbf{r},t)$ are much smaller than the wavelength of normal electromagnetic waves at the same frequency in the sample. Electromagnetic propagation effects are thus neglected by this approximation. A detailed account of this magnetostatic approximation is given in Appendix A.

It is important to note here that the spin wave theory discussed in this chapter and magnetostatic and magnetoexchange wave theories which are discussed elsewhere in this book are based on the magnetostatic approximation. Some previous works have incorrectly implied that the magnetostatic approximation is only used for magnetostatic mode theory. It applies equally well to higher-k spin wave excitations for which

exchange effects are important.

In principle, the dipole field $\mathbf{h}_{dip}(\mathbf{r},t)$ can be rigorously solved from Maxwell equations together with appropriate electromagnetic boundary conditions. For short wavelength spin waves, however, surface boundary conditions may be neglected and the problem is greatly simplified. This is because, for short wavelengths, there are so many oscillations along the sample surface that the effects of the surface fields average to zero. These considerations apply for $k \gg 2\pi/d$, where d is a nominal sample dimension. The situation in which k is comparable or less than $2\pi/d$ is treated in various theories for magnetostatic modes and magneto-exchange modes, which are not covered by this chapter (for a review article see, for example, Patton [13]).

In the spin wave model, the dipole field is expanded as a Fourier series according to

$$\mathbf{h}_{dip}(\mathbf{r},t) = \mathbf{h}_0(t) + \sum_{k \neq 0} \mathbf{h}_k(t)\, e^{-i\mathbf{k}\cdot\mathbf{r}} \ . \tag{2-13}$$

The $\mathbf{h}_0(t)$ term denotes the spatially uniform part of $\mathbf{h}_{dip}(\mathbf{r},t)$ connected with $\mathbf{m}_0(t)$. The $\mathbf{h}_k(\mathbf{r},t)$ terms denote the spatially nonuniform part of $\mathbf{h}_{dip}(\mathbf{r},t)$ connected with $\mathbf{m}_k(t)$ spin waves. The $\mathbf{h}_0(t)$ term is simply the demagnetizing field associated with $\mathbf{m}_0(t)$.

$$\mathbf{h}_0(t) = -4\pi\, \mathbf{N}\cdot\mathbf{m}_0(t) \ . \tag{2-14}$$

The nonuniform dipole field $\mathbf{h}_k(\mathbf{r},t)$ for $k \gg 2\pi/d$ derives from Maxwell equations as [11]

$$\mathbf{h}_k(t) = -4\pi\, \frac{\mathbf{k}}{k^2}[\mathbf{k}\cdot\mathbf{m}_k(t)] = -4\pi\, \mathbf{N}_k\cdot\mathbf{m}_k(t) \ . \tag{2-15}$$

The dipole tensor $\mathbf{N}_k$ is defined by the 3×3 matrix

$$\mathbf{N}_k = \frac{1}{k^2}\begin{pmatrix} k_x^2 & k_xk_y & k_xk_z \\ k_yk_x & k_y^2 & k_yk_z \\ k_zk_x & k_zk_y & k_z^2 \end{pmatrix}, \tag{2-16}$$

where the k_x, k_y, and k_z components are related to the wavenumber k and the angles θ_k and ϕ_k defined in Fig. 2-3.

$$k_x = k\, \sin\theta_k\, \cos\phi_k \ . \tag{2-17a}$$

$$k_y = k\, \sin\theta_k\, \sin\phi_k \ . \tag{2-17b}$$

$$k_z = k\, \cos\theta_k \ . \tag{2-17c}$$

This dipole tensor will play a important role in the analysis which follows. Because of the special role of $m_{kz}(t)$ terms in the nonlinear theory, it is convenient to separate the

$\mathbf{N}_k$ matrix into two parts, one which contains the first two columns,

$$\mathbf{N}_k^L = \frac{1}{k^2}\begin{pmatrix} k_x^2 & k_x k_y & 0 \\ k_y k_x & k_y^2 & 0 \\ k_z k_x & k_z k_y & 0 \end{pmatrix}, \tag{2-18}$$

and one with the last column only,

$$\mathbf{N}_k^N = \frac{1}{k^2}\begin{pmatrix} 0 & 0 & k_x k_z \\ 0 & 0 & k_y k_z \\ 0 & 0 & k_z^2 \end{pmatrix}. \tag{2-19}$$

Terms in $\mathbf{h}_k(t)$ deriving from the $\mathbf{N}_k^L \cdot \mathbf{m}_k(t)$ product contain only the linear $m_{kx}(t)$ and $m_{ky}(t)$ terms. However, terms deriving from the $\mathbf{N}_k^N \cdot \mathbf{m}_k(t)$ product contain $m_{kz}(t)$ terms, which bring in second order terms in $m_{0x}(t)\, m_{ky}(t)$ and $m_{0y}(t)\, m_{kx}(t)$. These nonlinear terms will contribute to the nonlinear equation of motion for spin wave instability.

The fifth field in $\mathbf{H}_{\text{eff}}(\mathbf{r},t)$ is the exchange field. The exchange field $\mathbf{h}_{\text{ex}}(\mathbf{r},t)$ is an effective field in the classical spin wave theory which models the effect of the quantum-mechanical exchange interaction on the dynamic response of the spin system. This effective exchange field can be expressed in terms of the spatial variation of the dynamic magnetization vector $\mathbf{m}(\mathbf{r},t)$ [11] (for a detailed derivation, see Lax and Button [14]).

$$\mathbf{h}_{\text{ex}}(\mathbf{r},t) = \frac{D}{M_s}\nabla^2 \mathbf{m}(\mathbf{r},t) = -\frac{D}{M_s}\sum_{k\neq 0} k^2\, \mathbf{m}_k(t)\, e^{-i\mathbf{k}\cdot\mathbf{r}}. \tag{2-20}$$

Here D is the exchange parameter, on the order of 5.4×10^{-9} Oe·cm^2 for YIG material. It is important to note that $\mathbf{h}_{\text{ex}}(\mathbf{r},t)$ is not a Maxwellian field. It does not enter directly into Maxwell equations.

The total effective field $\mathbf{H}_{\text{eff}}(\mathbf{r},t)$ is finally given by

$$\mathbf{H}_{\text{eff}}(\mathbf{r},t) = H_{int}\,\mathbf{e}_z + \mathbf{h}_p(t) - 4\pi\,\mathbf{N}\cdot\mathbf{m}_0(t) - 4\pi\sum_{k\neq 0}\mathbf{N}_k\cdot\mathbf{m}_k(t)\,e^{-i\mathbf{k}\cdot\mathbf{r}} - \frac{D}{M_s}\sum_{k\neq 0} k^2\,\mathbf{m}_k(t)\,e^{-i\mathbf{k}\cdot\mathbf{r}}. \tag{2-21}$$

Terms in this expression for the total effective field can be classified temporally or spatially. From the time variation point of view, $\mathbf{H}_{\text{eff}}(\mathbf{r},t)$ contains static and dynamic terms; while from the spatial variation point of view, $\mathbf{H}_{\text{eff}}(\mathbf{r},t)$ has uniform and nonuniform terms.

2.3. Equation of Motion

Having written down the detailed expressions for the magnetization vector $\mathbf{M}(\mathbf{r},t)$ and the total effective field $\mathbf{H}_{\text{eff}}(\mathbf{r},t)$, we now proceed to examine the equation of motion for the dynamic magnetization $\mathbf{m}(\mathbf{r},t)$. Substitution of $\mathbf{H}_{\text{eff}}(\mathbf{r},t)$ from Eq. (2-21) and $\mathbf{M}(\mathbf{r},t)$ from Eqs. (2-3) and (2-4) yields

$$\dot{\mathbf{m}}_0(t) + \sum_{k\neq 0} \dot{\mathbf{m}}_k(t)\, e^{-i\mathbf{k}\cdot\mathbf{r}}$$

$$= -|\gamma| \left[M_s \mathbf{e}_z + \mathbf{m}_0(t) + \sum_{k\neq 0} \mathbf{m}_k(t)\, e^{-i\mathbf{k}\cdot\mathbf{r}} \right] \times \left[H_{int}\, \mathbf{e}_z + \mathbf{h}_p(t) - 4\pi\, \mathbf{N}\cdot\mathbf{m}_0(t) \right.$$

$$\left. - 4\pi \sum_{k'\neq 0} \mathbf{N}_{k'} \cdot \mathbf{m}_{k'}(t)\, e^{-i\mathbf{k}'\cdot\mathbf{r}} - \frac{D}{M_s} \sum_{k'\neq 0} k'^2\, \mathbf{m}_{k'}(t)\, e^{-i\mathbf{k}'\cdot\mathbf{r}} \right]. \tag{2-22}$$

The dots above the $\mathbf{m}_0(t)$ and $\mathbf{m}_k(t)$ terms denote time derivatives. Equation (2-22) provides the foundation for investigating various linear and nonlinear spin wave processes. In particular, the analysis yields the uniform mode FMR response, spin wave dispersion, and spin wave instability thresholds. Virtually the whole of classical micromagnetic spin wave theory can be derived from this equation.

Closed form solutions to the above general equation of motion are extremely difficult or perhaps even impossible to obtain because of the nonlinearity involved in the problem. However, the equation can be restructured according to the order of different terms: linear terms involving the uniform mode $\mathbf{m}_0(t)$ terms only, linear terms involving spin wave $\mathbf{m}_k(t)$ terms only, second order terms involving $m_{0x,y}(t)\, m_{kx,y}(t)$ terms, and higher order nonlinear terms. Spin wave processes are analyzed by including different order terms and solving the various versions of these equations step by step.

We start by separating the general equation into two equations, one for $\mathbf{m}_0(t)$ and one for $\mathbf{m}_k(t)$. Note also that we will use only the x- and y-components of these two vector equations. The equation of motion for the uniform mode $\mathbf{m}_0(t)$ is given by

$$\dot{\mathbf{m}}_0(t) = -|\gamma| \left\{ [H_{int}\, \mathbf{m}_0(t) + 4\pi M_s \mathbf{N}\cdot\mathbf{m}_0(t) - M_s\, \mathbf{h}_p(t)] \times \mathbf{e}_z \right.$$

$$+ [4\pi\, \mathbf{N}\cdot\mathbf{m}_0(t) - \mathbf{h}_p(t)] \times \mathbf{m}_0(t) + 4\pi \sum_{k\neq 0} \mathbf{N}_k \cdot \mathbf{m}_k(t) \times \mathbf{m}_{-k}(t)$$

$$\left. + \frac{D}{M_s} \sum_{k\neq 0} k^2\, \mathbf{m}_k(t) \times \mathbf{m}_{-k}(t) \right\}. \tag{2-23}$$

Equation (2-23) contains linear terms as well as higher order terms. Although we will need to include nonlinear terms in the $\mathbf{m}_k(t)$ equation to deal with spin wave instability, we will not consider further the nonlinear terms in the $\mathbf{m}_0(t)$ equation. As shown by Suhl [8] and Schlömann [9], these terms are needed to obtain the steady state uniform

mode response above threshold. The linearized equation of motion for the uniform mode is given by

$$\dot{\mathbf{m}}_0(t) = -|\gamma|\left[H_{int}\,\mathbf{m}_0(t) + 4\pi M_s\,\mathbf{N}\cdot\mathbf{m}_0(t) - M_s\,\mathbf{h}_p(t)\right]\times\mathbf{e}_z\ . \tag{2-24}$$

This linear equation for the uniform mode $\mathbf{m}_0(t)$ yields the condition for ferromagnetic resonance and the basic uniform mode response. These analyses are developed in Sec. 3.1.

The general equation of motion for spin waves to all orders can be separated out from Eq. (2-22) as

$$\begin{aligned}\dot{\mathbf{m}}_k(t) = -|\gamma|\Big\{&\left[H_{int}\,\mathbf{m}_k(t) + 4\pi M_s\,\mathbf{N}_k\cdot\mathbf{m}_k(t) + Dk^2\,\mathbf{m}_k(t)\right]\times\mathbf{e}_z\\ &+ \left[4\pi\,\mathbf{N}\cdot\mathbf{m}_0(t) - \mathbf{h}_p(t) - \frac{D}{M_s}k^2\,\mathbf{m}_0(t)\right]\times\mathbf{m}_k(t)\\ &+ 4\pi\,\mathbf{N}_k\cdot\mathbf{m}_k(t)\times\mathbf{m}_0(t) + 4\pi\sum_{k'\neq 0,\,k}\mathbf{N}_{k'}\cdot\mathbf{m}_{k'}(t)\times\mathbf{m}_{k-k'}(t)\\ &+ \frac{D}{M_s}\sum_{k'\neq 0,\,k}k'^2\,\mathbf{m}_{k'}(t)\times\mathbf{m}_{k-k'}(t)\Big\}\ .\end{aligned} \tag{2-25}$$

The linearized equation of motion for spin waves is given by taking the first right-hand-side term only,

$$\dot{\mathbf{m}}_k(t) = -|\gamma|\left[H_{int}\,\mathbf{m}_k(t) + 4\pi M_s\,\mathbf{N}_k^L\cdot\mathbf{m}_k(t) + Dk^2\,\mathbf{m}_k(t)\right]\times\mathbf{e}_z\ . \tag{2-26}$$

This linearized equation will be solved in Sec. 3.2 for the spin wave normal modes and the corresponding dispersion relation.

The effect of the nonlinear coupling between the uniform mode and spin waves can be examined if we also retain first order terms of the form $m_{0x,y}(t)\,m_{kx,y}(t)$. The spin wave equation of motion to first order in the $\mathbf{m}_k(t)$ terms is then given by

$$\begin{aligned}\dot{\mathbf{m}}_k(t) = -|\gamma|\Big\{&\left[H_{int}\,\mathbf{m}_k(t) + 4\pi M_s\,\mathbf{N}_k^L\cdot\mathbf{m}_k(t) + Dk^2\,\mathbf{m}_k(t)\right]\times\mathbf{e}_z\\ &+ 4\pi M_s\,\mathbf{N}_k^N\cdot\mathbf{m}_k(t)\times\mathbf{e}_z + 4\pi\,\mathbf{N}_k^L\cdot\mathbf{m}_k(t)\times\mathbf{m}_0(t) - \mathbf{h}_p(t)\times\mathbf{m}_k(t)\Big\}\ .\end{aligned} \tag{2-27}$$

This nonlinear equation yields the so-called "first order" spin wave instability effect which is the main topic of this chapter. We will not discuss in this chapter other nonlinear effects resulting from the inclusion of higher order nonlinear coupling terms in the equation of motion. Such couplings eventually lead to additional instability effects and chaotic behaviors in magnetic systems (see, for example, [15-21]).

3. Linear Response Theory

3.1. Uniform Mode and Ferromagnetic Resonance

Before we discuss instability effects in ferrites, it is important to look at the linear response. The linear response of the uniform mode can be examined by linearizing the $\mathbf{m}_0(t)$ equation of motion, as given by Eq. (2-24). This linearized equation, in component form, is given below.

$$\dot{m}_{0x}(t) = -|\gamma|\,(H_{int} + 4\pi M_s N_y)\, m_{0y}(t) + |\gamma|\, M_s\, h_{py}(t)\ . \tag{3-1a}$$

$$\dot{m}_{0y}(t) = |\gamma|\,(H_{int} + 4\pi M_s N_x)\, m_{0x}(t) - |\gamma|\, M_s\, h_{px}(t)\ . \tag{3-1b}$$

First consider the pump-free response for $\mathbf{m}_0(t)$. For $\mathbf{h}_p(t)=0$, the general solution to Eq. (3-1) is given by

$$m_{0x}(t) = m_{0x}\cos(\omega_0 t + \varphi_0)\ , \tag{3-2a}$$

$$m_{0y}(t) = m_{0y}\sin(\omega_0 t + \varphi_0)\ . \tag{3-2b}$$

The above solution shows that the dynamic magnetization $\mathbf{m}_0(t)$ precesses elliptically around the direction of the static external field in the Larmor sense at the frequency ω_0 given by

$$\omega_0 = |\gamma|\sqrt{\left[H_{ext} + 4\pi M_s (N_x - N_z)\right]\left[H_{ext} + 4\pi M_s (N_y - N_z)\right]}\ . \tag{3-3}$$

This is the well known Kittel resonance frequency [2,3]. The φ_0 terms in Eq.(3-2) denotes an arbitrary initial phase. The z-component of $\mathbf{m}_0(t)$, according to Eq. (2-7a), contains only high order terms and is, therefore, zero in the linear limit. The ratio of the amplitude components m_{0x} and m_{0y} is found to be

$$\frac{m_{0x}}{m_{0y}} = \sqrt{\frac{H_{ext} + 4\pi M_s (N_y - N_z)}{H_{ext} + 4\pi M_s (N_x - N_z)}}\ . \tag{3-4}$$

This shows that for the uniform mode in an ellipsoid, the magnetization vector precesses elliptically around the static external field at frequency ω_0. For the special case of a sphere with $N_x=N_y=N_z=1/3$, the x- and y-components of the amplitude become equal,

$$m_{0x} = m_{0y}\ . \tag{3-5}$$

The precession is, therefore, circular and the frequency is simply

$$\omega_0 = |\gamma| H_{ext}\ . \tag{3-6}$$

Now consider the pumped response of $\mathbf{m}_0(t)$. We consider spherical samples only and assume that the uniform mode is driven by a microwave field $\mathbf{h}_p(t)$ at frequency ω_p. To better understand the physics of the uniform mode, we start with the simplest case which involves a circularly polarized microwave pumping field in the Larmor sense. We then examine the case involving a linearly polarized pumping which simulates the real situation in most experiments. For samples of ellipsoidal shape and subject to an arbitrary pumping configuration, the uniform mode response is more complicated [22].

We first consider the case of circular pumping for spheres. The microwave field is taken to be perpendicular to the static external field and circularly polarized in the Larmor sense with an amplitude h_p^+.

$$h_{px}(t) = h_p^+ \cos(\omega_p t) \ . \tag{3-7a}$$

$$h_{py}(t) = h_p^+ \sin(\omega_p t) \ . \tag{3-7b}$$

The linear response of the uniform mode for spheres is found from Eq. (3-1).

$$m_{0x}(t) = \chi_0^+ h_p^+ \cos(\omega_p t) \ . \tag{3-8a}$$

$$m_{0y}(t) = \chi_0^+ h_p^+ \sin(\omega_p t) \ , \tag{3-8b}$$

In the above, χ_0^+ specifies the Larmor susceptibility response.

$$\chi_0^+ = \frac{|\gamma| M_s}{\omega_0 - \omega_p} \ . \tag{3-9}$$

It is clear from Eq. (3-9) that the resonant response of the uniform mode occurs when the pump frequency coincides with the Kittel frequency, $\omega_p = \omega_0$. For this reason, the Kittel frequency ω_0 is usually termed the resonance frequency of the uniform precession mode, or ferromagnetic resonance (FMR) frequency.

As shown above, for the sphere case currently under consideration, the amplitudes m_{0x} and m_{0y} are equal. In this situation, it is convenient to define a reduced complex amplitude for the uniform mode.

$$\alpha_0(t) = \frac{1}{M_s} [m_{0x}(t) + i\, m_{0y}(t)] \ . \tag{3-10}$$

From Eq. (3-8), the linear response of the reduced uniform mode complex amplitude can be written as

$$\alpha_0(t) = \alpha_0^+ e^{i\omega_p t} \ , \tag{3-11}$$

with the Larmor component given by

$$\alpha_0^+ = \frac{|\gamma| h_p^+}{\omega_0 - \omega_p} . \tag{3-12}$$

We now turn to the linear pumping case for spheres. The microwave pumping field is taken to be linearly polarized and applied in the x-direction.

$$h_{px}(t) = h_p \cos(\omega_p t) . \tag{3-13a}$$

$$h_{py}(t) = 0 . \tag{3-13b}$$

Different from the circularly polarized pumping case, the uniform mode solution for Eq. (3-1) now contains both the Larmor and anti-Larmor components.

$$\alpha_0(t) = \alpha_0^+ e^{i\omega_p t} + \alpha_0^- e^{-i\omega_p t} . \tag{3-14}$$

For spheres, the Larmor and anti-Larmor amplitudes are given by

$$\alpha_0^+ = \frac{1}{2} \frac{|\gamma| h_p}{\omega_0 - \omega_p} \tag{3-15a}$$

and

$$\alpha_0^- = \frac{1}{2} \frac{|\gamma| h_p}{\omega_0 + \omega_p} . \tag{3-15b}$$

The Larmor part of the response, α_0^+, is the same as in Eq. (3-12), but with h_p^+ replaced by $h_p/2$, the amplitude of the Larmor part of the linear pump field. It is clear from the equations above that under the linear pumping the Larmor component contributes to the resonance when the pumping frequency ω_p is close to the Kittel frequency ω_0, while the anti-Larmor response is nonresonant. Even in the off-resonance situation, the Larmor component plays the dominant role. The above expression for $\alpha_0(t)$ will be used later in the instability theory for spin waves. It is worth noting that the form of the uniform mode response in Eq. (3-14) is general and not limited to the simple case of spheres under a linearly polarized pumping as considered here. The expressions of the Larmor and anti-Larmor components of the uniform mode for an ellipsoid under an arbitrarily polarized pumping are given in [22].

3.2. Spin Wave Dispersion

We now turn to discuss the linear response of spin waves. We examine the equation of motion for the spin wave amplitude $\mathbf{m}_k(t)$. The component form of the linearized equation of motion for $\mathbf{m}_k(t)$ can be obtained from Eq. (2-26).

$$\dot{m}_{kx}(t) = -\frac{1}{2}\,\omega_M \sin^2\theta_k \sin 2\phi_k\, m_{kx}(t) - (\omega_H + |\gamma| Dk^2 + \omega_M \sin^2\theta_k \sin^2\phi_k)\, m_{ky}(t)\ . \tag{3-16a}$$

$$\dot{m}_{ky}(t) = (\omega_H + |\gamma| Dk^2 + \omega_M \sin^2\theta_k \cos^2\phi_k)\, m_{kx}(t) + \frac{1}{2}\,\omega_M \sin^2\theta_k \sin 2\phi_k\, m_{ky}(t)\ . \tag{3-16b}$$

Here, we have introduced two important frequency parameters, ω_H and ω_M.

$$\omega_H = |\gamma|\, H_{int}\ . \tag{3-17a}$$

$$\omega_M = |\gamma|\, 4\pi M_s\ . \tag{3-17b}$$

These parameters express the internal field H_{int} and the magnetic saturation induction $4\pi M_s$ in frequency units. These two frequency parameters will be used extensively in the rest of this chapter.

In order to solve Eq. (3-16), we follow the approach of Suhl [8] and Schlömann [9]. As in the $\mathbf{m}_0(t)$ analysis, it is convenient to define two reduced complex amplitudes for spin waves.

$$\alpha_k(t) = \frac{1}{M_s}\,[m_{kx}(t) + i\, m_{ky}(t)]\ . \tag{3-18a}$$

$$\alpha^*_{-k}(t) = \frac{1}{M_s}\,[m_{kx}(t) - i\, m_{ky}(t)]\ . \tag{3-18b}$$

The spin wave equation of motion for $m_{kx}(t)$ and $m_{ky}(t)$ given in Eq. (3-16) can be transformed into a coupled matrix equation for $\alpha_k(t)$ and $\alpha^*_{-k}(t)$.

$$\frac{d}{dt}\begin{pmatrix}\alpha_k(t)\\ \alpha^*_{-k}(t)\end{pmatrix} = i\begin{pmatrix}A_k & B_k\\ -B^*_k & -A_k\end{pmatrix}\begin{pmatrix}\alpha_k(t)\\ \alpha^*_{-k}(t)\end{pmatrix}\ . \tag{3-19}$$

The A_k and B_k coefficients in the above equation are given by

$$A_k = \omega_H + |\gamma| Dk^2 + \frac{1}{2}\,\omega_M \sin^2\theta_k \tag{3-20a}$$

and

$$B_k = \frac{1}{2}\,\omega_M \sin^2\theta_k\, e^{i2\phi_k} \,. \tag{3-20b}$$

Note that A_k and B_k expressions are unchanged if the wavevector **k** is replaced by -**k**. Hence, the relations $A_{-k}=A_k$ and $B_{-k}=B_k$ are satisfied. These connections will be needed later.

Equation (3-19) shows that $\alpha_k(t)$ and $\alpha_{-k}^*(t)$ behave as a pair of coupled harmonic oscillators. Through a proper linear transformation, the normal modes of this coupled mode pair and their corresponding frequencies can be obtained. Such a transformation for spin waves was developed by Holstein and Primakoff [23]. The same transformation occurs in other physical problems and is also known as Bogoliubov transformation [24]. The details of the specific transformation procedure for spin waves and a physical interpretation based on the work of Kemanis and Wang [25] and Helszajn [26,27] are given in Appendix B. The coupled spin wave equation of motion for the $\alpha_k(t)$ and $\alpha_{-k}^*(t)$ of Eq. (3-19), decoupled under the Holstein-Primakoff transformation, yields

$$\frac{d}{dt}\begin{pmatrix} b_k(t) \\ \\ b_{-k}^*(t) \end{pmatrix} = i \begin{pmatrix} \omega_k & 0 \\ \\ 0 & -\omega_k \end{pmatrix} \begin{pmatrix} b_k(t) \\ \\ b_{-k}^*(t) \end{pmatrix} . \tag{3-21}$$

The ω_k parameter in Eq. (3-21) is

$$\omega_k^2 = A_k^2 - |B_k|^2 \,. \tag{3-22}$$

The Holstein-Primakoff transformation from the nondiagonal $[\alpha_k(t),\ \alpha_{-k}^*(t)]$ modes to the diagonal $[b_k(t),\ b_{-k}^*(t)]$ modes is given by

$$\begin{pmatrix} b_k(t) \\ \\ b_{-k}^*(t) \end{pmatrix} = \begin{pmatrix} \lambda_k & \mu_k \\ \\ \mu_k^* & \lambda_k \end{pmatrix} \begin{pmatrix} \alpha_k(t) \\ \\ \alpha_{-k}^*(t) \end{pmatrix} . \tag{3-23}$$

The λ_k and μ_k parameters are the Holstein-Primakoff transformation parameters developed in Appendix B.

$$\lambda_k = \sqrt{(A_k + \omega_k)/(2\,\omega_k)} \,. \tag{3-24a}$$

$$\mu_k = \sqrt{(A_k - \omega_k)/(2\,\omega_k)}\; e^{i2\phi_k} \,. \tag{3-24b}$$

Equation (3-21) has simple uncoupled harmonic oscillator solutions of the form

$$b_k(t) = b_k\, e^{i\omega_k t}\,, \tag{3-25a}$$

$$b^*_{-k}(t) = b^*_{-k}\, e^{-i\omega_k t}\,. \tag{3-25b}$$

These $b_k(t)$ and $b^*_{-k}(t)$ correspond to the spin wave normal modes at frequency ω_k. The explicit expression of frequency ω_k for these spin wave normal modes is given by

$$\omega_k = |\gamma| \sqrt{(H_{ext} - 4\pi M_s N_z + Dk^2)\,(H_{ext} - 4\pi M_s N_z + Dk^2 + 4\pi M_s \sin^2\theta_k)}\,. \tag{3-26}$$

This is the well known dispersion relation for spin waves [11, 28].

The above dispersion relation is a key result from the spin wave theory. The spin wave frequency ω_k depends on the wavevector $\mathbf{k}$ in several critical ways. First, ω_k increases more-or-less quadratically with wavenumber k. This increase comes from exchange energy. Second, ω_k increases with θ_k. This is a result of the dipole fields and energy associated with the nonzero $\nabla \cdot \mathbf{m}$ for $\theta_k \neq 0^o$ spin waves. Finally, we note that ω_k approaches certain limiting frequencies in the $k=0$ limit. For $\theta_k=0^o$ and $k=0$, we obtain

$$\omega_k(\theta_k=0^\circ,\ k=0) = \omega_H\,. \tag{3-27}$$

For $\theta_k=90^o$ and $k=0$, we obtain

$$\omega_k(\theta_k=90^\circ,\ k=0) = \omega_B\,, \tag{3-28}$$

with

$$\omega_B = \sqrt{\omega_H(\omega_H + \omega_M)}\,. \tag{3-29}$$

The ω_B parameter is important and finds extensive use in this chapter.

The spin wave dispersion ω_k vs. k is shown schematically in Fig. 3-1. Due to the symmetry involved in Eq. (3-26), we only need to study spin wave modes with $0^o \le \theta_k \le 90^o$. The result is a band of dispersion curves bounded by the $\theta_k=0^o$ and $\theta_k=90^o$ dispersion branches. Curves for $0^o < \theta_k < 90^o$ are contained inside the band. These dispersion curves represent spin wave states (k,θ_k,ω_k) which form the "spin wave manifold." As mentioned earlier, the spin wave frequency ω_k increases with the angle θ_k. Spin waves that propagate perpendicular to the static field ($\theta_k=90^o$) have a higher frequency than the spin waves that propagate parallel to the static field ($\theta_k=0^o$). The "bottom" of the band at $k=0$ limit is at ω_H. The "top" of the band at $k=0$ limit is at ω_B.

Two conclusions can be drawn from the linear response theory. First, ferromagnetic resonance of the uniform mode under the external microwave pumping is a linear effect and the resonance condition is given by $\omega_p=\omega_0$. Second, the spin wave modes precess elliptically with a frequency spectrum which may be represented by the continuum spin wave manifold shown in Fig. 3-1.

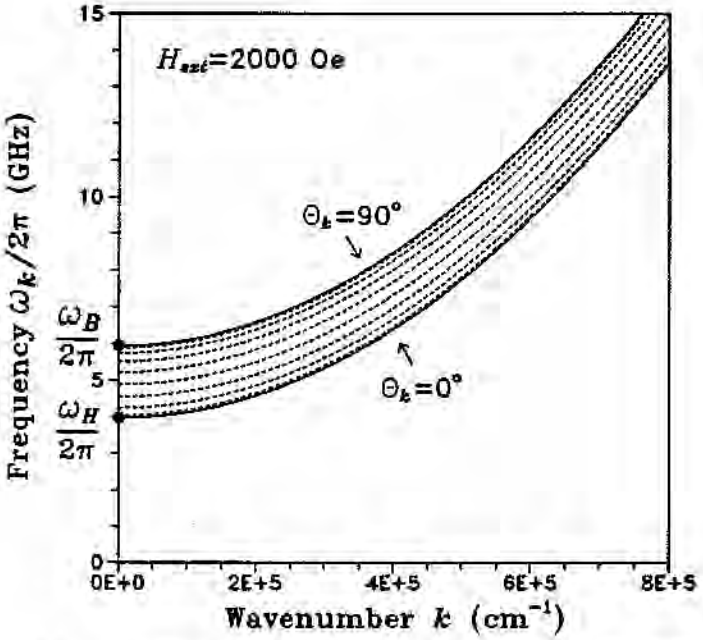

Figure 3-1 Spin wave frequency ω_k as a function of wavenumber k as the spin wave polar angle θ_k increases from 0° to 90° in 10° increments.

4. Spin Wave Instability Processes

In the previous section, we examined the linear response theory for both the uniform mode and spin waves. From the linear analysis, the FMR condition and spin wave spectrum were obtained. We now consider the nonlinear effects which are the focus of this chapter, spin wave instability processes. As briefly noted in the introduction, an instability theory for spin waves was first developed by Suhl [8] to explain high power microwave phenomena observed in ferrites, such as subsidiary absorption and premature saturation. The theory was later extended by Schlömann [9] to include additional high power effects, such as FMR foldover and parallel pumping instability. As already indicated, we will consider first order processes only.

4.1. Spin Wave Equation of Motion

Let us reexamine the $\mathbf{m}_k(t)$ equation of motion, paying particular attention to the additional first order nonlinear terms which lead to spin wave instability. The general equation to all orders is given by Eq. (2-25). The linear spin wave equation, limited to terms involving single $\mathbf{m}_k(t)$ factors only, is given by Eq. (2-26). Spin wave instability theory derives from the inclusion of additional terms which are *still* first order in the $\mathbf{m}_k(t)$ components but *also* contain $\mathbf{m}_0(t)$ components and/or a nonzero z-component of $\mathbf{h}_p(t)$, $h_{pz}(t)$. A z-component microwave pump field $h_{pz}(t)$ leads to a special case of

instability termed parallel pumping. The first order nonlinear $\mathbf{m}_k(t)$ equation for spin waves is given in vector form in Eq. (2-27). We now rewrite this equation in component form.

$$\begin{aligned}\dot{m}_{kx}(t) = &-(\omega_H + |\gamma| Dk^2 + \omega_M \sin^2\theta_k \sin^2\phi_k)\, m_{ky}(t) \\ &-\frac{1}{2}\omega_M \sin^2\theta_k \sin 2\phi_k\, m_{kx}(t) + \frac{1}{2}(\omega_M/M_s)\sin 2\theta_k \\ &\times [\sin\phi_k\, m_{0x}(t)\, m_{kx}(t) + \cos\phi_k\, m_{0y}(t)\, m_{kx}(t) \\ &+ 2\sin\phi_k\, m_{0y}(t)\, m_{ky}(t)] - |\gamma| h_{pz}(t)\, m_{ky}(t)\,. \end{aligned} \tag{4-1a}$$

$$\begin{aligned}\dot{m}_{ky}(t) = &(\omega_H + |\gamma| Dk^2 + \omega_M \sin^2\theta_k \cos^2\phi_k)\, m_{kx}(t) \\ &+\frac{1}{2}\omega_M \sin^2\theta_k \sin 2\phi_k\, m_{ky}(t) - \frac{1}{2}(\omega_M/M_s)\sin 2\theta_k \\ &\times [2\cos\phi_k\, m_{0x}(t)\, m_{kx}(t) + \sin\phi_k\, m_{0x}(t)\, m_{ky}(t) \\ &+ \cos\phi_k\, m_{0y}(t)\, m_{ky}(t)] + |\gamma| h_{pz}(t) m_{kx}(t)\,. \end{aligned} \tag{4-1b}$$

These two equations are the basis for first order spin wave instability theory. Equations (4-1a,b) constitute a coupling between the uniform mode $\mathbf{m}_0(t)$ or a parallel pump field $h_{pz}(t)$ and a spin wave mode $\mathbf{m}_k(t)$. In order to solve these two coupled equations, we follow the approach of Suhl [8] and Schlömann [9]. The equations are first reorganized by invoking the reduced complex spin wave amplitudes $\alpha_k(t)$ and $\alpha_{-k}^*(t)$ defined in Eq. (3-18). The resulting spin wave equation of motion for the $\alpha_k(t)$ and $\alpha_{-k}^*(t)$ is then obtained as

$$\frac{d}{dt}\begin{pmatrix}\alpha_k(t)\\ \alpha_{-k}^*(t)\end{pmatrix} = i\begin{pmatrix}A_k & B_k\\ -B_k^* & -A_k\end{pmatrix}\begin{pmatrix}\alpha_k(t)\\ \alpha_{-k}^*(t)\end{pmatrix} + i\begin{pmatrix}C_k(t) & D_k(t)\\ -D_k^*(t) & -C_k^*(t)\end{pmatrix}\begin{pmatrix}\alpha_k(t)\\ \alpha_k^*(t)\end{pmatrix}. \tag{4-2}$$

The A_k and B_k coefficients are the same as in the linear theory discussed in Sec. 3.2. The $C_k(t)$ and $D_k(t)$ coefficients are given by

$$C_k(t) = -\frac{1}{2}\,\omega_M \sin\theta_k \cos\theta_k\,[\,e^{-i\phi_k}\,\alpha_0(t) + e^{i\phi_k}\,\alpha_0^*(t)] + |\gamma| h_{pz}(t)\ , \tag{4-3a}$$

$$D_k(t) = -\,\omega_M \sin\theta_k \cos\theta_k\ e^{i\phi_k}\,\alpha_0(t)\ . \tag{4-3b}$$

The key new result here is in the $C_k(t)$ and $D_k(t)$ terms. These terms involve the uniform mode amplitude $\alpha_0(t)$ and the z-component of the microwave pumping field $h_{pz}(t)$. Under low power conditions, the $\alpha_0(t)$ and $h_{pz}(t)$ terms are small. In this limit, these terms may be neglected and Eq. (4-2) reduces to the linear form obtained in the previous section. As shown in Appendix B, the linear part of Eq. (4-2) can be diagonalized by a Holstein-Primakoff transformation. In order to solve Eq. (4-2), we proceed by applying the same transformation to the nonlinear equation with the $\alpha_0(t)$ and $h_{pz}(t)$ terms included. Under the Holstein-Primakoff transformation, Eq. (4-2) becomes

$$\frac{d}{dt}\begin{pmatrix} b_k(t) \\ \\ b_{-k}^*(t) \end{pmatrix} = i\begin{pmatrix} \omega_k + F_k(t) & G_k(t) \\ \\ -G_k^*(t) & -[\omega_k + F_k(t)]^* \end{pmatrix}\begin{pmatrix} b_k(t) \\ \\ b_{-k}^*(t) \end{pmatrix}. \tag{4-4}$$

The $F_k(t)$ and $G_k(t)$ coefficients are given by

$$F_k(t) = \lambda_k^2\, C_k(t) + |\mu_k|^2\, C_k^*(t) - \lambda_k \mu_k^*\, D_k(t) - \lambda_k \mu_k\, D_k^*(t) \tag{4-5a}$$

and

$$G_k(t) = -\,\lambda_k \mu_k \left[C_k(t) + C_k^*(t)\right] + \lambda_k^2\, D_k(t) + \mu_k^2\, D_k^*(t)\ . \tag{4-5b}$$

Here, the parameters λ_k and μ_k are the Holstein-Primakoff transformation parameters developed in Appendix B and given by Eq. (3-23).

The $F_k(t)$ term in Eq. (4-4) leads to a change in the spin wave frequency ω_k. This change is typically small compared with the value of ω_k when the microwave frequency ω_p is far away from the FMR frequency ω_0. In the first order spin wave instability processes of concern here, this off-resonance condition is always satisfied. Therefore, the $F_k(t)$ term may be ignored.

The $G_k(t)$ term in Eq. (4-4) has a more substantial effect. As we shall see, this term leads to the parametric coupling and unstable growth of the spin wave amplitudes $b_k(t)$ and $b_{-k}^*(t)$ at high pumping power levels. As will be shown shortly, the $G_k(t)$ term turns out to be the coupling coefficient for the energy pumped into the spin wave modes through the microwave field and the uniform mode.

4.2. First Order Spin Wave Instability

To study first order instability effects of the sort introduced above, it is necessary to introduce dissipation in the magnetic system. This is done phenomenologically by

replacing the uniform mode frequency ω_0 and spin wave frequency ω_k in Eqs. (4-4) and (4-5) with complex frequencies.

$$\omega_0 \rightarrow \Omega_0 = \omega_0 + i\eta_0 \ . \tag{4-6a}$$

$$\omega_k \rightarrow \Omega_k = \omega_k + i\eta_k \ . \tag{4-6b}$$

Here, η_0 denotes the uniform precession relaxation rate, and η_k denotes spin wave relaxation rate for the particular spin wave wavevector **k** under consideration. The uniform precession relaxation rate is conveniently expressed in terms of the corresponding FMR linewidth. For the uniform precession, the resonance absorption half-power full field-swept linewidth ΔH is expressed in terms of η_0.

$$\Delta H = \frac{2\eta_0}{|\gamma|} \ . \tag{4-7a}$$

For spin waves, we write a parallel expression,

$$\Delta H_k = \frac{2\eta_k}{|\gamma|} \ , \tag{4-7b}$$

where ΔH_k is simply defined as the spin wave full linewidth. Strictly speaking, this parameter is not a linewidth. It simply expresses the spin wave relaxation rate in linewidth units.

The spin wave equation of motion with the $F_k(t)$ term neglected and damping parameters included is given by

$$\frac{d}{dt}\begin{pmatrix} b_k(t) \\ \\ b_{-k}^*(t) \end{pmatrix} = i\begin{pmatrix} \Omega_k & G_k(t) \\ \\ -G_k^*(t) & -\Omega_k^* \end{pmatrix}\begin{pmatrix} b_k(t) \\ \\ b_{-k}^*(t) \end{pmatrix} . \tag{4-8}$$

Our objective now is to solve this equation for $b_k(t)$ and $b_{-k}^*(t)$, and obtain corresponding threshold conditions for instability. We follow the approach of Schlömann [9]. The $G_k(t)$ term is first expanded into a series,

$$G_k = \sum_n G_k^{(n)} e^{in\omega_p t} \ . \tag{4-9}$$

First order instability can be evaluated by considering only the n=1 term of Eq. (4-9), that is, that part of $G_k(t)$ which varies as $\exp(i\omega_p t)$. The algebra of this selection rule will be evident shortly. Similarly, second order instability is obtained by considering the n=2 term, although this case is not included in this chapter. The spin wave equation of motion pertinent to first order instability is given by

$$\frac{d}{dt}\begin{pmatrix} b_k(t) \\ \\ b^*_{-k}(t) \end{pmatrix} = i \begin{pmatrix} \Omega_k & G_k^{(1)} e^{i\omega_p t} \\ \\ -G_k^{(1)^*} e^{-i\omega_p t} & -\Omega_k^* \end{pmatrix} \begin{pmatrix} b_k(t) \\ \\ b^*_{-k}(t) \end{pmatrix} . \tag{4-10}$$

The $G_k^{(1)}$ expression for linearly polarized microwave field is given by

$$G_k^{(1)} = -\frac{\omega_M}{4\omega_k} \sin^2\theta_k e^{i2\phi_k} |\gamma| h_{pz} - \frac{\omega_M}{2\omega_k} \sin\theta_k \cos\theta_k e^{i2\phi_k}$$

$$\times \left[(\omega_H + |\gamma| Dk^2 + \omega_k) e^{-i\phi_k} \alpha_0^+ + (\omega_H + |\gamma| Dk^2 - \omega_k) e^{i\phi_k} \alpha_0^{-*} \right] . \tag{4-11}$$

Note that $G_k^{(1)}$, h_{pz}, α_0^+, and α_0^- are time independent. The parallel pumping field is given by $h_{pz}(t)=h_{pz}\cos(\omega_p t)$. The α_0^+ and α_0^- are the uniform mode Larmor and anti-Larmor responses discussed in Sec. 3. From Eq. (4-10), we obtain an ordinary differential equation for $b_k(t)$,

$$\left\{ \frac{d^2}{dt^2} + (2\eta_k - i\omega_p) \frac{d}{dt} + \left[\omega_k^2 + \eta_k^2 - \omega_p(\omega_k + i\eta_k) - |G_k^{(1)}|^2 \right] \right\} b_k(t) = 0 . \tag{4-12}$$

The general solution to Eq. (4-12) is given by

$$b_k(t) = b_k e^{i\frac{1}{2}\omega_p t + \kappa t} . \tag{4-13}$$

The time exponential κ-parameter in this solution is obtained as

$$\kappa = -\eta_k \pm \sqrt{|G_k^{(1)}|^2 - (\omega_k - \omega_p/2)^2} . \tag{4-14}$$

Equations (4-13) and (4-14) reveal the basic nature of first order spin wave instability processes. One has, essentially, a competition between the coupling of microwave energy into the b_k mode via $G_k^{(1)}$ and relaxation of energy out of the b_k mode via η_k. For a spin wave at low power levels, where $G_k^{(1)}$ is negligible, Eq. (4-13) reduces to the linear solution discussed above with an additional damping term.

$$b_k(t) = b_k e^{i\omega_k t - \eta_k t} . \tag{4-15}$$

The spin wave amplitude remains at thermal levels due to the relaxation losses. At higher power levels where $|G_k^{(1)}| > |\omega_k - \omega_p/2|$ is satisfied, the spin wave amplitude increases exponentially with time as described by Eq. (4-13) and we have instability.

We see, therefore, that the κ-parameter determines the instability condition. When $\kappa<0$ is satisfied, losses dominate and spin wave amplitude is stable and remains at

thermal levels. This is the low power case. When the power is high enough so that $\kappa>0$ is satisfied, the coupling dominates, the spin wave is unstable, and $b_k(t)$ tends to grow exponentially in time. The condition $\kappa=0$ marks the onset of spin wave instability. The instability threshold condition is obtained from the $\kappa=0$ condition, which yields

$$|G_k^{(1)}| = \sqrt{(\omega_k - \omega_p/2)^2 + \eta_k^2} \quad . \tag{4-16}$$

We can now see the significance of $\omega_p/2$ and the specific nature of the threshold. The smallest value of the coupling term $|G_k^{(1)}|$ for Eq. (4-16) occurs at $\omega_k=\omega_p/2$. This frequency condition describes the coupling of the microwave pump field or the uniform precession mode at ω_p to spin waves at $\omega_k=\omega_p/2$ and $\pm\mathbf{k}$. The threshold condition now reduces to a very simple equation,

$$|G_k^{(1)}| = \eta_k \quad . \tag{4-17}$$

Recall that $|G_k^{(1)}|$, given in Eq. (4-11), contains field amplitude parameters of microwave pump in h_{pz} for parallel pumping and in h_p through $\alpha_0^{\pm}$ for perpendicular pumping. The main point for now is that $|G_k^{(1)}|$ increases linearly with the microwave pump field amplitude h_{pz} and h_p. At the critical point in h_{pz} or h_p where Eq. (4-17) is satisfied, instability occurs and the corresponding h_{pz} or h_p is the microwave field threshold amplitude h_c for that instability. In the parallel pumping case, we have $h_p=0$. In this limit, one may solve Eq. (4-17) for h_{pz} and obtain a microwave field threshold amplitude h_c for the parallel pumping instability of specific spin waves. One may follow the same procedure for the perpendicular pumping case ($h_{pz}=0$) and obtain the subsidiary absorption threshold h_c. We will deal with the specific situations for parallel pumping and subsidiary absorption in Sections 5 and 6 below. A general oblique pumping configuration is also possible [22, 29-32].

In summary, we have discussed the general theory of first order instability for spin waves. Depending on the configuration of the microwave field and the static external field applied to the sample, the instability effects can be categorized as parallel pumping, perpendicular pumping, or oblique pumping. In the following two sections, we will discuss specific instability processes for the parallel pumping and the perpendicular pumping configurations.

5. Parallel Pumping Instability

The instability effect considered first is for the parallel pumping configuration. This is the simplest case in the first order spin wave instability theory. As discussed in Sec. 2, the uniform mode can not be directly excited by a microwave field applied parallel to the static external field direction. At high power levels, however, spin wave instability still occurs. The existence of this instability effect was predicted theoretically by Schlömann [9] and Morgenthaler [33,34], and first observed by Schlömann, Green, and Milano [35].

5.1. Parallel Pumping Instability Threshold

The theory developed in Sec. 4 for first order spin wave instability shows that spin wave instability occurs as the magnitude of the coupling term $G_k^{(1)}$ in the spin wave equation of motion exceeds the spin wave relaxation rate η_k. For the parallel pumping case, we have $h_p=0$, $\alpha_0^+=0$, and $\alpha_0^-=0$. The microwave pumping field $h_{pz}(t)$ is applied along the static external field direction and taken as

$$h_{pz}(t) = h_{pz}\cos(\omega_p t) \ . \tag{5-1}$$

Under these conditions, the magnitude of the $G_k^{(1)}$ coupling term of Eq. (4-11) becomes

$$|G_k^{(1)}| = \frac{\omega_M}{4\omega_k}\sin^2\theta_k\,|\gamma|\,h_{pz} \ . \tag{5-2}$$

The instability threshold amplitude h_c of a linearly polarized microwave pumping field for the specific ($\pm k$, θ_k, $\omega_k=\omega_p/2$) spin wave modes is then obtained from Eqs. (4-17) and (4-7b) as

$$h_c = \frac{\omega_p}{\omega_M}\frac{\Delta H_k}{\sin^2\theta_k} \ . \tag{5-3}$$

We emphasize that this threshold h_c is not yet the observed threshold in experiments, but simply the threshold for *specific* ($\pm k$, θ_k, $\omega_k=\omega_p/2$) spin wave mode pairs. Note that the spin wave dispersion for a given field H_{ext} and fixed ω_k yields a connection between k and θ_k. This connection is given by

$$\omega_H + |\gamma|Dk^2 = \sqrt{\omega_k^2 + \left(\frac{1}{2}\omega_M\sin^2\theta_k\right)^2} - \frac{1}{2}\omega_M\sin^2\theta_k \ . \tag{5-4}$$

We know from Appendix B that $(\omega_H+|\gamma|Dk^2)$ is given by $e_k\omega_k$, where e_k is the spin wave ellipticity factor. We may write, therefore,

$$\omega_H + |\gamma|Dk^2 = e_k(\theta_k)\,\omega_k \ , \tag{5-5a}$$

with

$$e_k(\theta_k) = \sqrt{1 + \left(\frac{\omega_M}{2\omega_k}\sin^2\theta_k\right)^2} - \frac{\omega_M}{2\omega_k}\sin^2\theta_k \ . \tag{5-5b}$$

These two equations, in combination with the $\omega_k=\omega_p/2$ condition, yield limits on k and θ_k for various field ranges, as will be discussed shortly.

The remaining step is to obtain the threshold which corresponds to experiment. This observable threshold is the *minimum* value of h_c for all *available* ($\pm k$, θ_k, $\omega_k=\omega_p/2$)

states for a given static field. We write

$$h_{crit} = \min_{k} \left\{ \frac{\omega_p}{\omega_M} \frac{\Delta H_k}{\sin^2\theta_k} \right\} \tag{5-6}$$

to designate this lowest value of h_c relative to the available (k, θ_k, $\omega_k=\omega_p/2$) states.

In order to calculate the minimum threshold h_{crit}, we first need to determine the ranges of k- and θ_k-values that are available at $\omega_k=\omega_p/2$ for a given static field. Figure 5-1 shows the spin wave manifold for three distinct static field values. Case (I) is for low fields, such that $\omega_B<\omega_k=\omega_p/2$ is satisfied. In this case, θ_k will range from 0° to 90° with k always nonzero. The available k-values at $\omega_k=\omega_p/2$ are indicated by the black bar on the k-axis for Case (I) in Fig. 5-1. The field region for Case (I) is given by

$$4\pi M_s N_z < H_{ext} < H_{90} . \tag{5-7}$$

Here, the lower field limit $4\pi M_s N_z$ is the static demagnetizing field for a saturated sample. The upper field limit H_{90} is the external field at which the spin wave frequency $\omega_k=\omega_p/2$ coincides with the frequency of the $\theta_k=90°$ branch of the manifold at the $k=0$ limit. This field limit is given by

$$H_{90} = 4\pi M_s (N_z - \frac{1}{2}) + \frac{1}{2}\sqrt{(\omega_p/|\gamma|)^2 + (4\pi M_s)^2} . \tag{5-8}$$

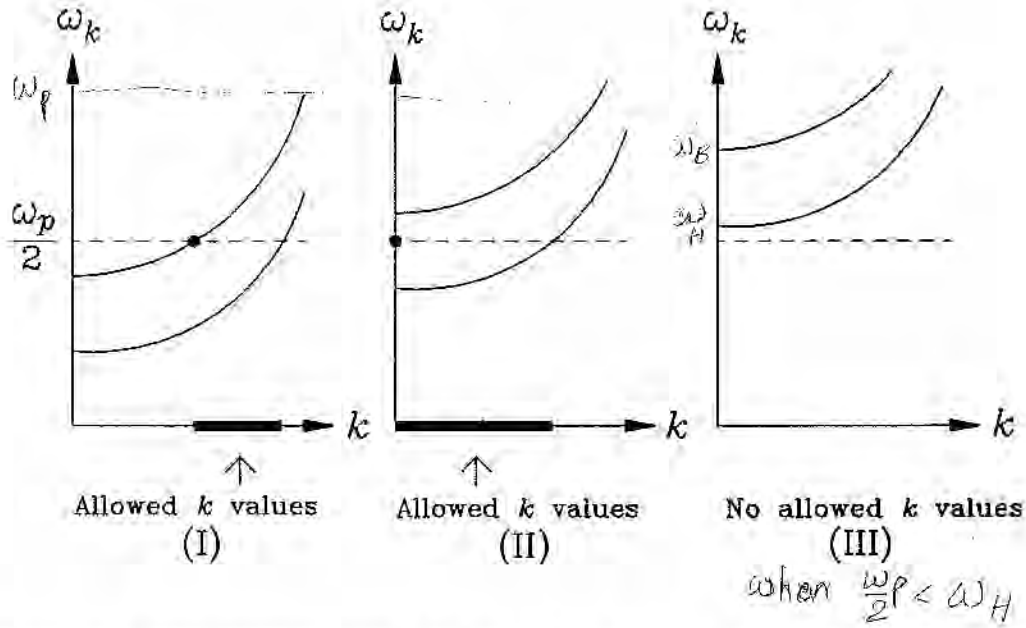

Figure 5-1 Spin wave manifold position relative to the half-pump frequency $\omega_p/2$ at (I) low, (II) intermediate, and (III) high static external field.

For a YIG sphere with saturation induction $4\pi M_s = 1750$ Gauss and an X-band pumping frequency, say $\omega_p/2\pi = 10$ GHz, this low field region corresponds to 580 Oe $< H_{ext} <$ 1680 Oe. We denote this range as Region I.

Case (II) is for intermediate fields such that $\omega_H < \omega_k = \omega_p/2 < \omega_B$ is satisfied. In this case, θ_k will range from 0° to some θ_k^{top} with $\theta_k^{top} < 90°$ and k will range from some k^{top} at $\theta_k = 0°$ to $k=0$ at $\theta_k = \theta^{top}$. The black bar for Case (II) extends down to $k=0$. The field region for Case (II) is given by

$$H_{90} < H_{ext} < H_0 \tag{5-9}$$

with

$$H_0 = \frac{\omega_p}{2|\gamma|} + 4\pi M_s N_z \,. \tag{5-10}$$

Here, the upper field limit H_0 is the static field at which the spin wave frequency $\omega_k = \omega_p/2$ coincides with the frequency of the $\theta_k = 0°$ branch of the manifold at the $k=0$ limit. For the same parameters given above, this intermediate field region corresponds to 1680 Oe $< H_{ext} <$ 2370 Oe. This field range is denoted as Region II.

For Case (III), in which the static field is high enough that $H_{ext} > H_0$ is satisfied, there are no spin waves available at $\omega_p/2$. The entire spin wave manifold is above the half pump frequency, $\omega_k > \omega_p/2$. This field limit H_0 is, therefore, the cut-off field for the first order the spin wave instability. In our example, this field region corresponds to $H_{ext} > 2370$ Oe. We denote this high field range as Region III.

We now evaluate the minimum threshold in each region, based on Eq. (5-6) and the available spin wave states for our three field regions depicted in Fig. 5-1. Strictly speaking, we need to minimize the $\Delta H_k/\sin^2\theta_k$ factor in h_{crit}, with the **k**-dependence of $\Delta H_k(\mathbf{k})$ included explicitly. For the moment, however, we will consider only the $1/\sin^2\theta_k$ factor for the minimization and take ΔH_k to be a **k**-independent constant. Following this discussion, we will then consider the effect of the spin wave linewidth **k**-dependence on the minimization procedure and the threshold h_{crit}.

From the $1/\sin^2\theta_k$ term in h_c, it is clear that the lowest h_c corresponds to the largest possible $\sin\theta_k$. We denote the (k, θ_k) mode with the lowest threshold as $(k_{crit}, \theta_k^{crit})$. As evident from Fig. 5-1 and the above discussion, the position of the spin wave manifold region, relative to $\omega_k = \omega_p/2$, determines the available k and θ_k values. In the low field Region I, the manifold at $k=0$ is well below $\omega_k = \omega_p/2$, all (k_{crit}, θ_k) modes are available and the lowest threshold is for $\theta_k^{crit} = 90°$ and k_{crit} as indicated by the solid circle in the left part of Fig. 5-1. As the field is increased, the manifold shifts upward, θ_k^{crit} remains at 90° and k_{crit} decreases. This situation continues as long as the field remains in Region I. We have $k_{crit} = [(H_{90} - H_{ext})/D]^{1/2}$, $\theta_k^{crit} = 90°$, and $h_{crit} = (\omega_p/\omega_M)\Delta H_k$ in this region. Note that h_{crit} is constant.

In field Region II, we have $H_{90} < H_{ext} < H_0$. The maximum θ_k is less than 90° and associated with $k=0$. From the spin wave dispersion equation for $\omega_k = \omega_p/2$ and $k=0$, we may write θ_k^{crit} explicitly for Region II as

$$\theta_k^{crit} = \sin^{-1}\sqrt{\frac{(H_0 - H_{ext})(\omega_H + \omega_p/2)}{4\pi M_s \omega_H}} \quad . \tag{5-11}$$

As the static external field ranges from H_{90} to H_0, the θ_k^{crit} ranges from 90° down to 0° and k_{crit} stays at zero, as indicated by the solid circle in the middle part of Fig. 5-1. Correspondingly, the threshold h_{crit} increases as θ_k^{crit} decreases and finally diverges at $\theta_k^{crit}=0°$ as H_{ext} approaches H_0. When the external field exceeds H_0, we enter Region III. In this high field region, as shown by the right part of Fig. 5-1, there are no modes degenerate with $\omega_k=\omega_p/2$, and h_{crit} remains at infinity.

Figure 5-2 shows some specific numerical results for the parallel pumping instability theory, along with the data from the original parallel pumping experiments of Schlömann, Green, and Milano [35] for a single crystal YIG sphere. The frequency was $\omega_p/2\pi=9.42$ GHz for both the theory and the data. The calculated curve of h_{crit} vs. H_{ext} in Fig. 5-2(a) and the corresponding k_{crit} vs. H_{ext} and θ_k^{crit} vs. H_{ext} curves in Fig. 5-2(b) are for $\Delta H_k=0.31$ Oe. This value of ΔH_k was used to match the theory to the data at the data minimum near $H_{ext}=1700$ Oe. A correction to H_{ext} of 80 Oe towards higher field was made for the theoretical curves to account for anisotropy field in the [100] magnetized single crystal YIG sphere in the experiment.

We will return to a discussion of the differences between the theory and the data in a moment. For now, we are concerned with the solid curves in Fig. 5-2. The distinct Region I and Region II behaviors discussed above are clearly evident. In Region I, h_{crit} is constant, θ_k^{crit} is constant at 90°, and k_{crit} gradually decreases to zero. In Region II, h_{crit} increases and diverges at $H_{ext}=H_0$, θ_k^{crit} decreases from 90° to 0°, and k_{crit} stays at zero.

Turn now to the data, shown by the solid circles in Fig. 5-2(a). The data show a distinct cusp and minimum h_{crit} value at the Region I/Region II boundary. The threshold values, however, do not match our simple theory for H_{ext} values either below or above this cusp point. As indicated above, the missing consideration is the **k**-dependence of the spin wave linewidth ΔH_k. It is evident from Fig. 5-2 that $\Delta H_k(\mathbf{k})$ has a substantial effect on the h_{crit} vs. H_{ext} profile. It is this effect that yields the cusp-like character at $H_{ext}=1700$ Oe evident from the data and the observed h_{crit} vs. H_{ext} behavior. The cusp has led to the naming of h_{crit} vs. H_{ext} profiles as "butterfly curves," a term first coined by LeCraw and Spencer and cited by Schlömann [36]. We conclude this discussion of parallel pumping with an analysis of this spin wave linewidth effect.

5.2. Spin Wave Linewidth Effect

It is clear from the above results that the assumption of a **k**-independent relaxation rate η_k and a corresponding constant ΔH_k does not lead to satisfactory agreement between theory and data for parallel pumping in single crystal YIG. We now consider the effect of including a **k**-dependent ΔH_k in the minimization procedure for h_{crit}. It is well known that the spin wave relaxation rate *is* **k**-dependent. Theoretical analyses by Sparks [37,

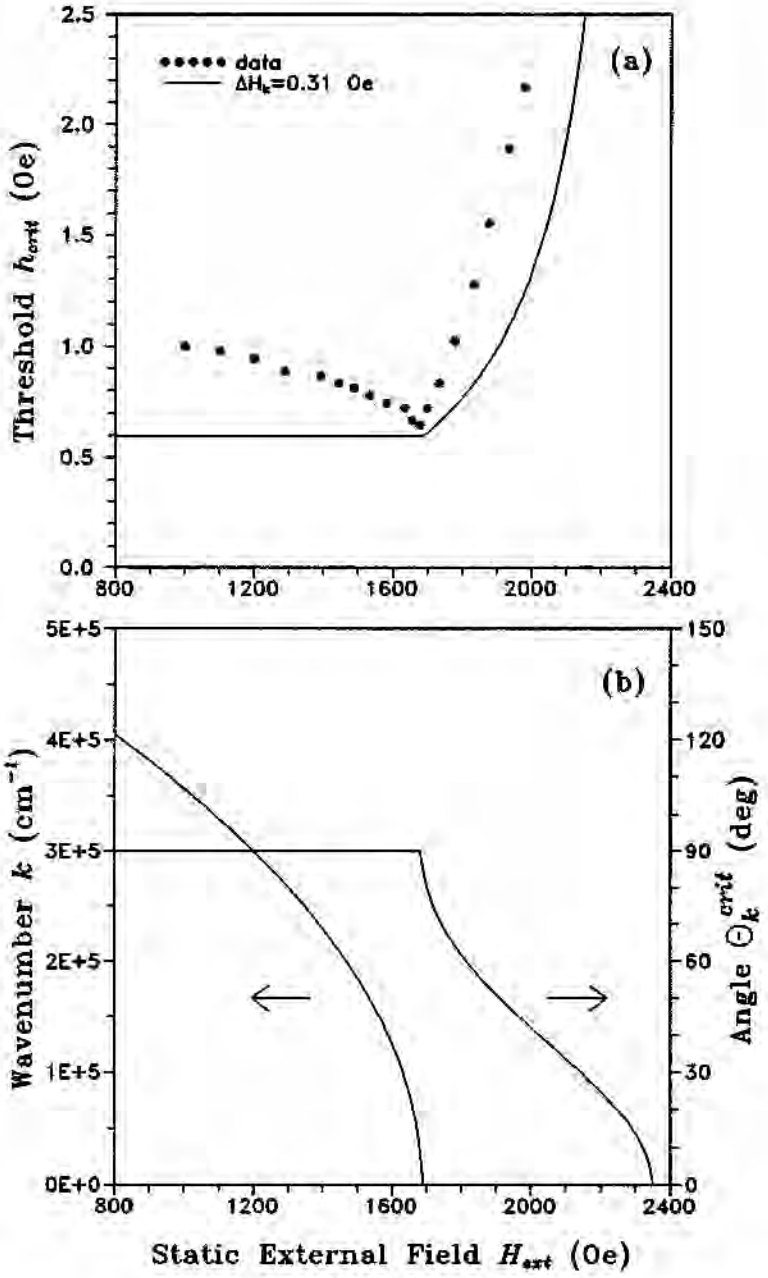

Figure 5-2 (a) Calculated threshold, along with the data of Schlömann *et al.* [35], and (b) wavenumber and polar angle vs. static field curves for parallel pumping instability.

38] provide information on possible k-dependences in various high and low k limits. These theoretical results led Patton [39, 40] and Patton and Jantz [41, 42] to propose various simple trial $\Delta H_k(\mathbf{k})$ functions to fit butterfly curves for various pumping configurations in single crystal YIG material. The simplest such function was

$$\Delta H_k(\mathbf{k}) = A_0 + A_1 \sin^2 2\theta_k + A_2 k \ . \qquad (5\text{-}12)$$

As we shall see, such a function works extremely well for parallel pumping. The physical significance of the terms in Eq. (5-12) are discussed by Sparks [38]. The main point for this discussion is that ΔH_k can have a significant **k**-dependence. As will be evident shortly, this **k**-dependence has an important effect on the parallel pumping butterfly curve obtained from theory.

Before going through specific numerical calculations which minimize $\Delta H_k(\mathbf{k})/\sin^2\theta_k$ for various values of the A_0, A_1, and A_2 parameters in Eq. (5-12) and yield theoretical butterfly curves which compare favorably with experimental results, we first consider the basic effect of the different terms in Eq. (5-12) on the threshold.

The constant term A_0 in the $\Delta H_k(\mathbf{k})$ expression determines the minimum value of the spin wave linewidth, and therefore the value of h_{crit} at the parallel pumping butterfly curve minimum. This point can be justified by the fact that $\Delta H_k(\mathbf{k})/\sin^2\theta_k$ is at its minimum when $k=0$ and $\theta_k=90^\circ$, and the minimum value is A_0. From the discussion given above for Fig. 5-1, it is clear that this threshold minimum condition occurs at $H_{ext}=H_{90}$ and $h_{crit}=A_0\omega_p/\omega_M$.

The influence of the A_1 and A_2 terms on the butterfly curve is more complicated. Figure 5-3 shows some theoretical butterfly curves calculated with various A_1 and A_2 combinations. It is clear that the inclusion of the A_1 and A_2 terms in the spin wave linewidth does yield a better fit to the data. The A_1 and A_2 terms play independent roles in parallel pumping case. Below the cusp position, we have $\theta_k^{crit}=90^\circ$ and the A_1 term is zero. The A_2 term yields an h_{crit} which decreases with increasing static field. Figure 5-3 shows the best fit to the data at fields below the cusp position is for $A_2=6\times10^{-7}$ Oe$\cdot$cm^{-1}. Above the cusp position, we have $k_{crit}=0$ and the A_2 term is zero. The A_1 angle term increases the h_{crit} for static fields above the cusp position. Figure 5-3 shows that the best fit to the data at fields above the cusp position is for $A_1=0.22$ Oe.

In spite of the above changes in h_{crit} which result from the inclusion of a k-dependent spin wave linewidth, the values of k_{crit} and θ_k^{crit} vs. H_{ext} for the minimum threshold modes are not affected and the curves in Fig. 5-2(b) still apply. This is because the k-dependent terms in Eq. (5-4), where applicable, serve only to increase the threshold. This will not be the case for the subsidiary absorption case to be discussed in the next section.

The above discussion has been limited to the case of isotropic magnetic insulators and spherical samples. There are additional instability effects in parallel pumping due to anisotropy, sample shape, and linewidth. Anisotropy effects in single crystals under parallel pumping are discussed in detail by Sethares *et al.* [43] and Patton [39, 40]. These effects relate to the variation in the $G_k^{(1)}$ coupling term with the azimuthal spin wave propagation angle ϕ_k under conditions of lower symmetry. Shape effects are discussed by Patton and Green [44]. There are also fine structure effects related to the discrete nature of the allowed spin wave modes first observed by Jantz and Schneider [45, 46]. A discussion of these effects is beyond the scope of this brief review.

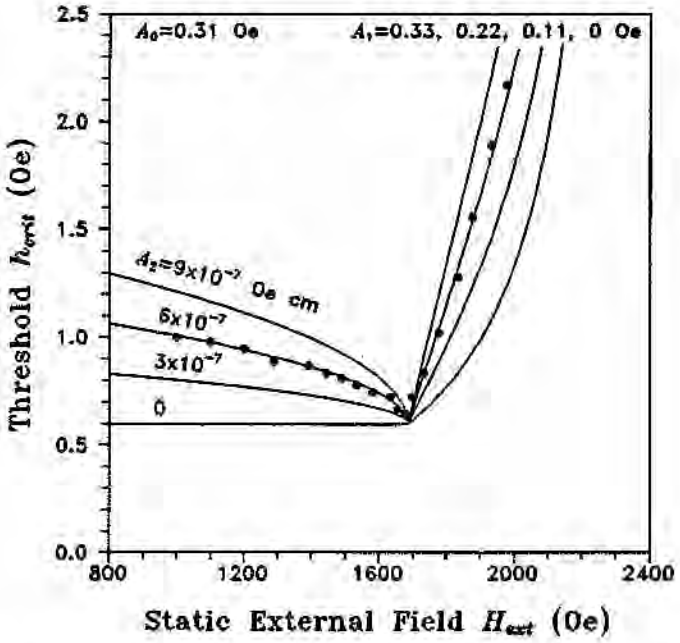

Figure 5-3 Butterfly curves calculated with a k-dependent ΔH_k for various A_1 and A_2 parameter combinations, along with the data of Schlömann *et al.* [35].

6. Subsidiary Absorption

In the last section, we discussed first order spin wave instability effect taking place at high power levels when a microwave pump field is applied to the sample along the static external field direction. We now consider first order spin wave instability effect associated with a microwave pumping field applied perpendicular to the static external field. As indicated in the Introduction, this perpendicular pumping instability effect was first observed by Bloembergen, Damon and Wang [4-7] in nickel ferrite spheres at 9 GHz as a broad absorption profile at fields lower than the FMR position. It was given the name "subsidiary absorption" by Suhl [47]. At lower frequencies, typically below 3 GHz for YIG material, it is possible to have first order instability at FMR. In effect, the subsidiary absorption field is coincident with the subsidiary absorption field [48-51]. In this discussion, however, we limit our consideration only to the case of a separate and distinct subsidiary absorption region.

6.1. Perpendicular Pumping Instability Threshold

As discussed earlier, first order spin wave instability occurs when the magnitude of the coupling term $G_k^{(1)}$ in Eq. (4-11) exceeds the spin wave relaxation rate η_k. For the perpendicular pumping case, we have $h_{pz}=0$, $h_p\neq 0$, $\alpha_0^+\neq 0$, and $\alpha_0^-\neq 0$. The $G_k^{(1)}$ term

in Eq. (4-11) is then given by

$$G_k^{(1)} = -\frac{\omega_M}{2\omega_k}\sin\theta_k\cos\theta_k e^{i2\phi_k}\left[(\omega_H + |\gamma|Dk^2 + \omega_k)\, e^{-i\phi_k}\alpha_0^+ + (\omega_H + |\gamma|Dk^2 - \omega_k)\, e^{i\phi_k}\alpha_0^{-*}\right]. \quad (6\text{-}1)$$

In this case, the coupling to spin waves derives indirectly from the microwave pump field through the uniform mode Larmor response α_0^+ and anti-Larmor response α_0^-. For a linearly polarized microwave pump field of amplitude h_p, the uniform mode response components α_0^+ and α_0^- of a sphere were obtained in Sec. 3.

$$\alpha_0^+ = \frac{1}{2}\frac{|\gamma|h_p}{\omega_0 - \omega_p}\,. \quad (6\text{-}2a)$$

$$\alpha_0^- = \frac{1}{2}\frac{|\gamma|h_p}{\omega_0 + \omega_p}\,. \quad (6\text{-}2b)$$

As indicated above, we are explicitly concerned with subsidiary absorption for fields well below the FMR position, such that $\omega_0 \ll \omega_p$ is satisfied. In this case, damping of the uniform mode has little effect on the response. In general, however, one should replace ω_0 with $\Omega_0=\omega_0+i\eta_0$ in order to include the effect of the uniform mode relaxation on $\alpha_0^{\pm}$ and the resulting threshold. This is important especially for lower frequencies, as already mentioned. In this chapter we will limit the discussion to the off-resonance situation in which $(\omega_p-\omega_0) \gg \eta_0$ is satisfied.

Equation (6-1) can be written explicitly in terms of ω_k, ω_p, ω_0, θ_k, and ϕ_k.

$$G_k^{(1)} = -\frac{1}{2}|\gamma|h_p\left(\frac{\omega_M}{2\omega_k}\right)e^{i2\phi_k}W(\omega_k, \theta_k, \phi_k)\,. \quad (6\text{-}3)$$

$$W(\omega_k, \theta_k, \phi_k) = \omega_k \sin\theta_k\cos\theta_k\left[\frac{e_k(\theta_k)+1}{\omega_0 - \omega_p}\, e^{-i\phi_k} + \frac{e_k(\theta_k)-1}{\omega_0 + \omega_p}\, e^{i\phi_k}\right]. \quad (6\text{-}4)$$

In the equation above, the spin wave dispersion is used to obtain the connection between k and θ_k as specified by Eq. (5-4). The $e_k(\theta_k)$ is the θ_k-dependent spin wave ellipticity function given by Eq. (5-5).

The instability threshold amplitude h_c of a linearly polarized pumping field for the *specific* ($\pm k$, θ_k, ϕ_k, $\omega_k=\omega_p/2$) spin wave modes is now given by

$$h_c = \frac{\omega_p}{\omega_M}\frac{\Delta H_k}{|W(\theta_k, \phi_k)|}\,. \quad (6\text{-}5)$$

Here, $W(\theta_k,\phi_k)$ denotes the W-function subject to the additional condition $\omega_k=\omega_p/2$. Recall that the range of available k- and θ_k-values at $\omega_k=\omega_p/2$ depends on the static field, according to Eq. (5-4). As in the parallel pumping instability case, the actual threshold which would be observed in a specific measurement for a given field H_{ext} and frequency ω_p is the *minimum* achievable value of h_c subject to the *available* k-, θ_k-, and ϕ_k-values for spin waves at $\omega_k=\omega_p/2$. We write

$$h_{crit} = \min_{\mathbf{k}} \left\{ \frac{\omega_p}{\omega_M} \frac{\Delta H_k}{|W(\theta_k, \phi_k)|} \right\} \tag{6-6}$$

to designate this minimum value of h_c relative to the available (k, θ_k, ϕ_k, $\omega_k=\omega_p/2$) modes for a given static field. In order to calculate the minimum threshold h_{crit}, we need to determine the ranges of k-, θ_k-, and ϕ_k-values that are available at $\omega_k=\omega_p/2$ for a given static field, similar to the procedure discussed in the last section for parallel pumping. In general, we must take both the denominator function with θ_k- and ϕ_k-dependence and the numerator function ΔH_k with full $\mathbf{k}$-dependence into account. Here, we will proceed as for parallel pumping. We will first consider the different field regions and the available (k, θ_k) states in these regions. We will then construct a subsidiary absorption butterfly curve for a $\mathbf{k}$-independent ΔH_k and make some initial comparisons with selected data. Finally, we will consider the effect of $\Delta H_k(\mathbf{k})$ on theoretical butterfly curve and use various choices for $\Delta H_k(\mathbf{k})$ to fit the theory to the data.

If ΔH_k is $\mathbf{k}$-independent, the $\mathbf{k}$-dependence of h_c enters only through the θ_k- and ϕ_k-dependent $W(\theta_k, \phi_k)$ function as specified by Eqs. (6-4) and (6-5). In order to minimize the threshold in this case, we look for the θ_k- and ϕ_k-values which *maximize* the denominator function. First consider the maximization of the $|W(\theta_k, \phi_k)|$ function with respect to ϕ_k. Recall that $[e_k(\theta_k)-1]$ is always negative. Note also that for subsidiary absorption, $(\omega_0-\omega_p)$ is also negative. Both the $[e_k(\theta_k)+1]/(\omega_0-\omega_p)$ and $[e_k(\theta_k)-1]/(\omega_0+\omega_p)$ terms in Eq. (6-4) are negative. Because of this same sign condition, the $|W(\theta_k, \phi_k)|$ function is maximized with respect to ϕ_k when the $\exp(\pm i\phi_k)$ factors in Eq. (6-4) are equal, that is, $\phi_k=0°$ or 180°. The $|W(\theta_k, \phi_k)|$ term now simplifies to a θ_k-dependent term only.

$$|W(\theta_k)| = \frac{1 + (\omega_0/\omega_p)\, e_k(\theta_k)}{1 - (\omega_0/\omega_p)^2} \sin\theta_k \cos\theta_k \ . \tag{6-7}$$

We can see immediately that $|W(\theta_k)|$ will be maximized with respect to θ_k at angles near $\theta_k=45°$. The ellipticity function serves to shift this maximum to slightly smaller θ_k values. Note that the equivalent $|W(\theta_k)|$ term for parallel pumping is simply $\sin^2\theta_k$, with a maximum at $\theta_k=90°$.

The minimum threshold field amplitude h_{crit} is now given by

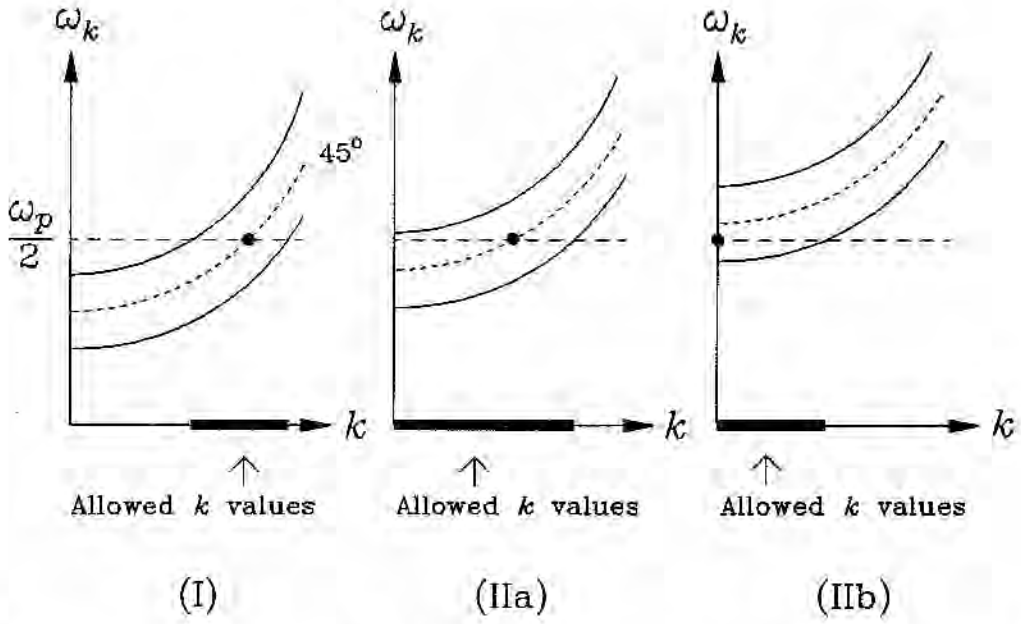

Figure 6-1 Spin wave manifold position relative to the half-pump frequency $\omega_p/2$ at (I) low and (IIa,b) intermediate static external field, as discussed in the text.

$$h_{crit} = \min_{\theta_k} \left\{ \frac{\omega_p}{\omega_M} \frac{1-(\omega_0/\omega_p)^2}{[1+(\omega_0/\omega_p)\, e_k(\theta_k)]} \frac{\Delta H_k}{\sin\theta_k \cos\theta_k} \right\} . \tag{6-8}$$

Recall that ω_0 is the FMR frequency, given by $\omega_0 = |\gamma| H_{ext}$ for spheres. The functional form of h_{crit} for perpendicular pumping given in Eq. (6-8) is more complicated than that for parallel pumping given in Eq. (5-6). As with the parallel pumping case, we look for the θ_k-value which *maximizes* the denominator function. For the low field Region I in Fig. 5-1 and repeated in Fig. 6-1, we may scan over the full range of θ_k, $0° \le \theta_k \le 90°$, as already discussed above. In the case of subsidiary absorption, however, the minimum threshold occurs at some $\theta_k^{crit} = \theta_k^{min} \approx 45°$ indicated by the solid circle in the left part of Fig. 6-1, as just discussed above.

For the intermediate field Region II, we will have the same $\theta_k^{crit} = \theta_k^{min} \approx 45°$ for that low-field part of the region for which θ_k^{top} exceeds θ_k^{min} as long as the allowed range for θ_k still includes θ_k^{min}. As we move up in field, still in Region II but such that θ_k^{top} falls below θ_k^{min}, θ_k^{crit} for the minimum threshold becomes θ_k^{top}. Region II therefore divides into two subregions, Region IIa for fields sufficiently low that θ_k^{top} is above θ_k^{min} and Region IIb for higher fields such that θ_k^{min} is above θ_k^{top}. The middle and right diagrams in Fig. 6-1 show these two cases. For Region IIa in the middle diagram, the solid circle is at θ_k^{min} and nonzero k. For Region IIb in the right diagram, the solid circle is at θ_k^{top} and $k=0$. For even higher fields, we move into Region III, and have no spin waves available at $\omega_k = \omega_p/2$, as shown before in Fig. 5-1. Region III is not

shown in Fig. 6-1.

Simply stated, we have two special θ_k-values, (1) θ_k^{min}, which maximizes the denominator function, $[1+(\omega_0/\omega_p)e_k(\theta_k)]\sin\theta_k\cos\theta_k$ over the full range of $0^o \le \theta_k \le 90^o$ and, hence, minimizes h_c, and (2) θ_k^{top}, which is simply the biggest value of θ_k that is allowed for specific values of H_{ext}, ω_p, ω_M, D, *etc.* The minimum threshold corresponds to whichever θ_k is smallest, θ_k^{min} or θ_k^{top}. We note that θ_k^{min} depends only on the FMR frequency ω_0, the pump frequency ω_p, and the magnetization through ω_M.

We now turn to discuss some specific quantitative results for subsidiary absorption, first for a **k**-independent ΔH_k and then with various **k**-dependences. The discussion parallels that for parallel pumping in Sec. 5. We make comparison with the data of Patton and Jantz [42] for a single crystal YIG sphere at pump frequency of $\omega_p/2\pi=9.16$ GHz. Figure 6-2 shows the minimum instability threshold h_{crit}, the wavenumber k_{crit}, and the polar angle θ_k^{crit} of the minimum threshold spin waves at $\omega_k=\omega_p/2$, calculated as a function of the static external field H_{ext} for a constant spin wave linewidth, $\Delta H_k=0.29$ Oe. This value of ΔH_k was chosen to match the minimum h_{crit} values from the theory to the lowest measured values. A correction to H_{ext} of 50 Oe towards lower field was made for the theoretical curves to account for anisotropy field in the [111] magnetized single crystal YIG sphere in the experiment.

It is clear from Fig. 6-2(a) that the match between the simple theory for a constant ΔH_k and the data is very bad. We will return to a discussion of the differences between the theory and the data shortly. For now, we are concerned with the solid curves. Figure 6-2(a) shows the calculated curve of the minimum threshold h_{crit} vs. static field H_{ext} for a YIG sphere with parameters specified above. Following the lore of parallel pumping, curves of this type in subsidiary absorption are also called "butterfly curves." The figure shows that the threshold decreases with increasing static field for field region 800 Oe$<H_{ext}<$1900 Oe. The threshold is minimum near $H_{ext}=1900$ Oe. At higher fields, the threshold increases rapidly and diverges at about 2200 Oe. The spin wave wavenumber k_{crit} and the polar angle θ_k^{crit} vs. static field for the minimum threshold spin waves are indicated in Fig. 6-2(b). At fields below about 1800 Oe, the minimum threshold modes have nonzero k_{crit} and $\theta_k^{crit}\approx 42^o$. The k_{crit} in this region decreases as increasing static field while θ_k^{crit} is nearly constant. This corresponds to our previously discussed field Region I and field Region IIa. At the field just above 1800 Oe, k_{crit} drops to zero. Above that field, k_{crit} remains at zero as θ_k^{crit} decreases from 42° to zero. This corresponds to field Region IIb. The cut-off field for $\omega_k=\omega_p/2$ spin waves is at 2170 Oe, the lower field limit for Region III.

There are two important differences between this subsidiary absorption "butterfly curve" and the corresponding parallel pumping counterpart. First, the minimum occurs at a somewhat higher value of H_{ext}. This increase is due to the change in the θ_k^{min} from 90° for parallel pumping case to near 45° for subsidiary absorption. Second, below the minimum position h_{crit} increases with decreasing field. In the parallel pumping case, the constant ΔH_k condition led to a constant h_{crit} in this region. The increase in instability threshold with decreasing field in this region for subsidiary absorption is due to the decrease in the uniform mode response as one moves lower in field and farther away

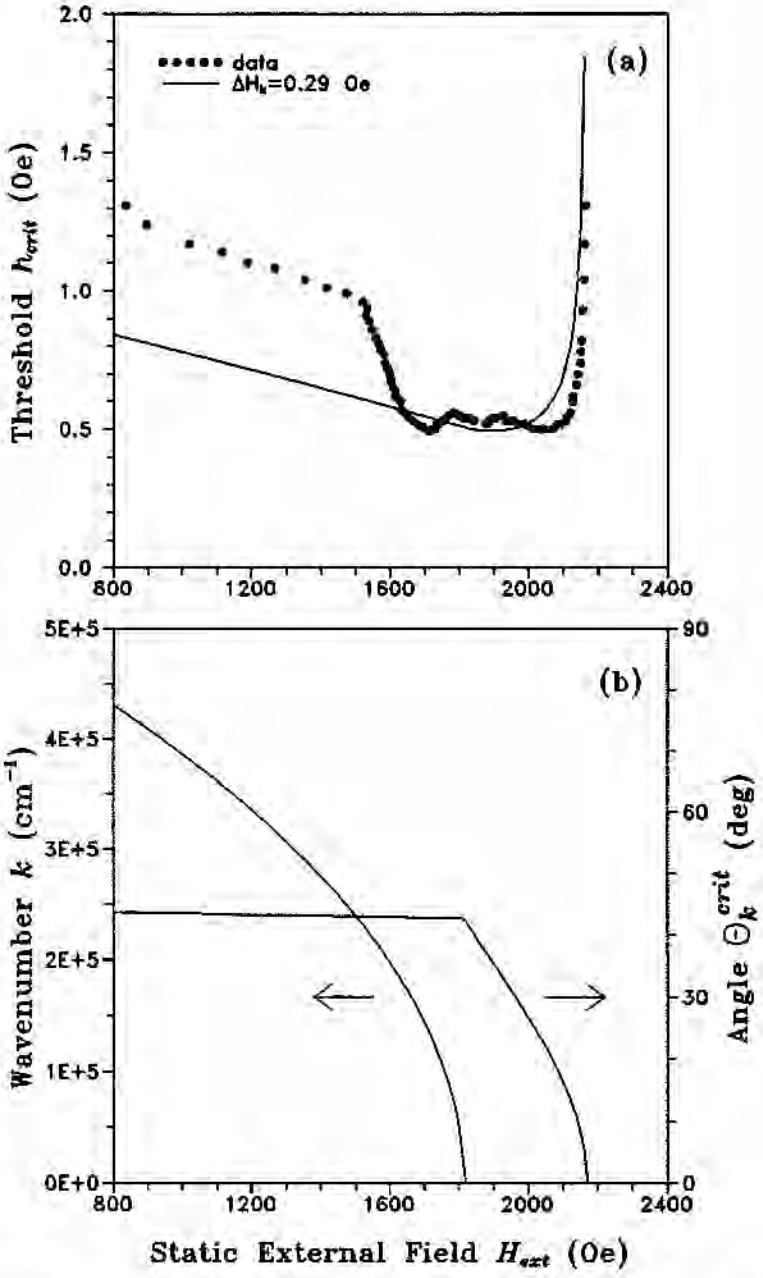

Figure 6-2 (a) Calculated threshold, along with the data of Patton and Jantz [42], and (b) wavenumber and polar angle vs. static field curves for subsidiary absorption.

from the FMR position. Recall that the uniform mode is not involved in the instability processes for parallel pumping.

Turn now to the data, shown by the solid circles in Fig. 6-2(a). The data show a rather complicated butterfly curve which is not at all compatible with the basic theoretical

result presented above. The differences include (1) a broad flat minimum in the field region around the theoretical butterfly curve minimum; (2) a fine structure superimposed upon this broad minimum; (3) a very rapid increase in h_{crit} at fields just below the broad minimum, followed by (4) a kink. Below the kink point, the increases in h_{crit} with decreasing field for both the data and the basic theory have about the same slopes.

These differences are substantial. With the exception of the fine structure, the differences can all be resolved by including a **k**-dependent spin wave linewidth function $\Delta H_k(\mathbf{k})$ in the minimization procedure to obtain h_{crit}. These effects are discussed below. The fine structure appears to be related to magnetostatic mode effects [42,52,53] or magnetoelastic interactions [54].

6.2. Spin Wave Linewidth Effect

This final section is devoted to the effect of the **k**-dependence of the spin wave linewidth on the butterfly curve for subsidiary absorption. The approach here is basically the same as in the parallel pumping analysis. We seek an suitable and physically plausible $\Delta H_k(\mathbf{k})$ function which can serve to match the theoretical h_{crit} to the data.

A reasonable starting point is to use the $\Delta H_k(\mathbf{k})$ function with a linear k-dependence which worked well for parallel pumping, given by Eq. (5-12) and repeated below.

$$\Delta H_k^{PP}(\mathbf{k}) = A_0 + A_1 \sin^2 2\theta_k + A_2 k \ . \tag{6-9}$$

Recall that the functional form of this $\Delta H_k(\mathbf{k})$ was determined empirically, guided by theoretical considerations and the results of various fits to data. Both a $\sin^2 2\theta_k$ dependence and a linear k-dependence are contained in the three-magnon confluence relaxation theory of Sparks *et al.* [37,38]. Figure 6-3 shows the same data as in Fig. 6-2 and already discussed, along with various theoretical curves generated with the spin wave linewidth function in Eq. (6-9). A very good fit to the high field part of the experimental butterfly curve is obtained for $A_0 = A_1 = 0.17$ Oe. The linear k-dependence which worked well for parallel pumping, however, does not work well for subsidiary absorption. If we use $A_2 = 0$ and, therefore, no k-dependence, the slope of the h_{crit} vs. H_{ext} curve at low field matches the data but the h_{crit} values are too low. If A_2 is increased we obtain a semblance of a kink at about the right value of H_{ext}, but the h_{crit} curves at external fields below the kink point increase much too rapidly. The dilemma here is that some k-dependence is needed to get here to the kink, but a linear k-dependence makes the h_{crit} at fields below the kink point too big and increase too rapidly with decreasing field.

The above results suggest that the k-dependence of ΔH_k needed to fit the subsidiary absorption data is some sort of step function in k which is zero at $k=0$ and constant when k is large. Such a function, in fact, is obtained from spin wave relaxation theory. The theory of Sparks *et al.* [37,38] for three-magnon confluence processes yields a spin wave relaxation rate given by

$$\eta_k \propto L(k/k_c) \ , \tag{6-10}$$

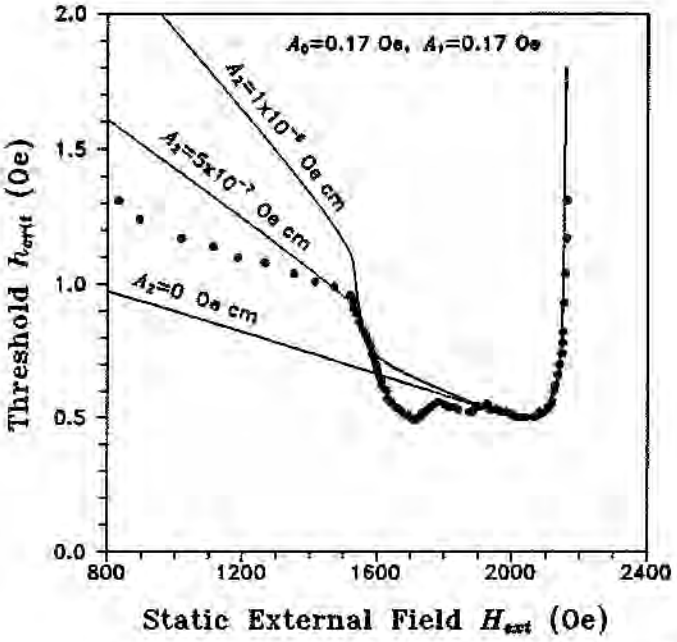

Figure 6-3 Theoretical fits to the butterfly curve data for a trial function which includes a linear k dependence in ΔH_k.

with the $L(x)$ function given by

$$L(x) = \frac{0.72}{x} \ln\left[1 + 8x^2 \frac{1 + 2x^2}{1 + 8x^2}\right]. \tag{6-11}$$

In the $x \ll 1$ limit, $L(x)$ is linear in x according to $L(x) \approx 5.8x$. The $L(x)$ has a maximum value of 1 at about $x=0.5$ and slowly decreases for larger values of x. Figure 6-4 shows the $L(x)$ function. The function goes to zero at $x=0$, is approximately linear in x for $x \leq 0.3$, and nearly flat at $L(x) \approx 1$ for $x \geq 0.5$. For a high value of k_c, $L(k/k_c)$ yields a linear k-dependence as needed to explain parallel pumping. A low value of k_c yields a step function of sorts in k, as needed for subsidiary absorption. Patton and Jantz [42] used this result to determine an operational $\Delta H_k(\mathbf{k})$ function for subsidiary absorption,

$$\Delta H_k^{SA}(\mathbf{k}) = A_0 + A_1 \sin^2 2\theta_k + B_1 L(k/k_c) . \tag{6-12}$$

Here, the coefficients A_0, A_1, B_1, and k_c are adjustable parameters.

A best fit theoretical butterfly curve calculated on the basis of this $\Delta H_k(\mathbf{k})$ function is shown in Fig. 6-5(a), along with the data already discussed in the above. The theoretical curve was obtained with $A_0=0.17$ Oe, $A_1=0.17$ Oe, $B_1=0.16$ Oe, and $k_c=10^5$ cm^{-1}. Except for the low field part of the flat region between 1600 and 1900 Oe, the quantitative agreement between the theory and the data is remarkable. Note that in the original paper of Patton and Jantz [42] the value of the fitted B_1 parameter was

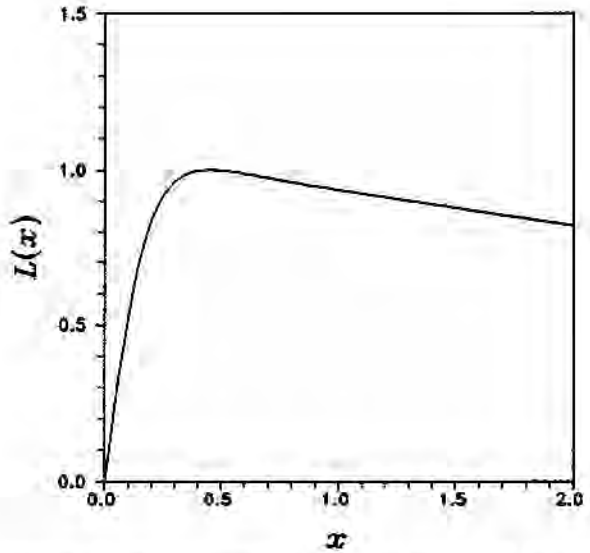

Figure 6-4 The function $L(x)$ in the three-magnon confluence theory of Sparks [38].

given incorrectly. The fitted value was the same as used here.

The relevant spin wave wavenumber k_{crit} and the polar angle θ_k^{crit} vs. H_{ext} curves for the minimum threshold spin waves are shown in Fig. 6-5(b). These dependences are quite different from those shown in Fig. 6-2(b). As the static field increases from the lowest values, the θ_k^{crit}-values initially remain at approximately 35° and the k_{crit}-values decrease with increasing field. This behavior continues until a kink point is reached at about 1550 Oe. As the field exceeds this kink value, k_{crit} drops abruptly to zero. This forces a jump in θ_k^{crit} up to about 75° for the $\omega_k=\omega_p/2$ spin waves. As the field is further increased, k_{crit} remains at zero and θ_k^{crit} decreases smoothly to $\theta_k=0°$ at cut-off near 2170 Oe.

The above kink effect and the abrupt jumps in k_{crit} and θ_k^{crit} at the kink field do not occur for a constant ΔH_k. They derive directly from the $L(k/k_c)$ term in Eq. (6-12). They can be explained in terms of a competition between the k-dependent $\Delta H_k(\mathbf{k})$ and the denominator function, $[1+(\omega_0/\omega_p)e(\theta_k)]\sin\theta_k\cos\theta_k$, in the minimization procedure.

When the static field is low, corresponding to Region I, there are no spin waves available at $k=0$. In this region, relatively little is gained by changing θ_k from the θ_k^{min} specified by our denominator function. The k-and θ_k-dependences in $\Delta H_k(\mathbf{k})$ do result in a small additional shift from $\theta_k \approx 42°$ to $\theta_k \approx 35°$.

The kink point is slightly higher in field than the Region I/Region II boundary. This relationship is important. Recall that as soon as the field enters Region II from Region I, spin wave states at $k=0$ become available. At some point, depending on the relative values of A_0, A_1, *etc.*, one gains more in reducing $\Delta H_k(\mathbf{k})$ by letting k go to zero than one loses due to the decrease in the $[1+(\omega_0/\omega_p)e(\theta_k)]\sin\theta_k\cos\theta_k$ coupling term. This cannot happen precisely at the Region I/Region II boundary because at that point, we would have $\theta_k=90°$ and zero coupling. At a somewhat higher field, however, a lower

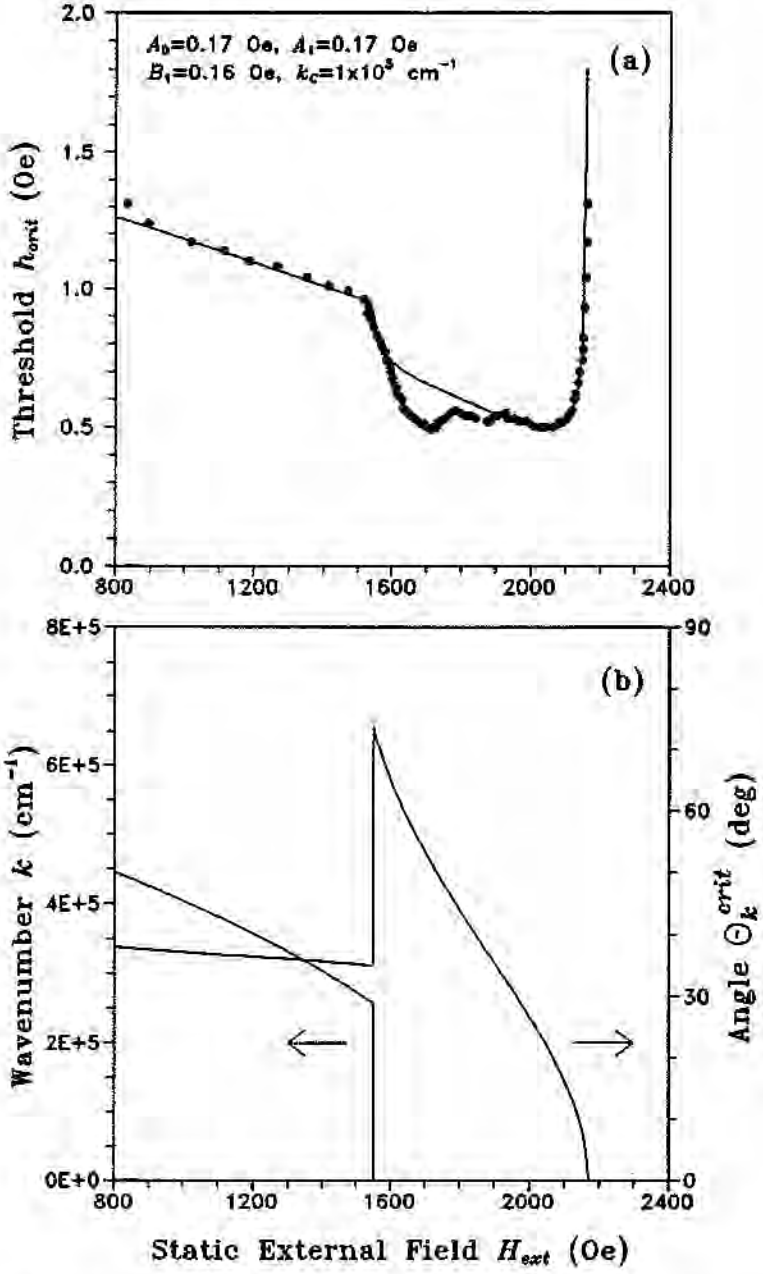

Figure 6-5 (a) A best fit theoretical butterfly curve to the data of Patton and Jantz [50] for a YIG sphere at 9.16 GHz, with (b) the corresponding spin wave wavenumber and the polar angle.

h_{crit} can be achieved by jumping to k=0. This is the origin of the kink. This jump effect is shown in Fig. 6-6.

Note that if A_0 were very large relative to A_1 and B_1, the effect on $\Delta H_k(\mathbf{k})$ by going to k=0 would have little effect. This is the case for polycrystalline ferrite materials,

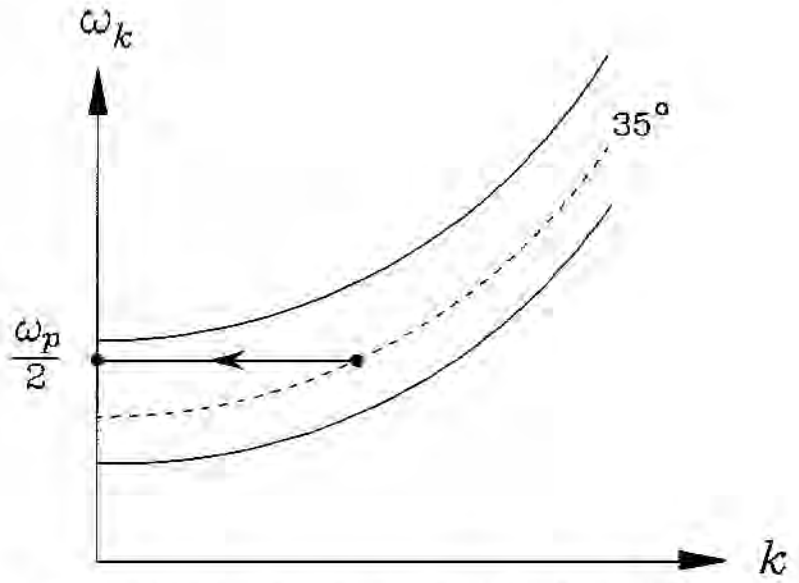

Figure 6-6 Schematic illustration of spin wave manifold under the kink field bias, as discussed in the text.

materials with large impurity levels, *etc.* In such cases, the measured butterfly curves are more like the one obtained earlier from the simple theory and shown by the $A_2=0$ curve in Fig. 6-3.

One remaining question concerns the complicated structure over the flat region from 1600 to 1900 Oe in the experimental butterfly curve, as shown in Fig. 6-3. This portion of the butterfly curve shows considerable structure, in the form of many dips, bumps, and kinks. The fits discussed above indicate that this field region corresponds to modes with $k\approx 0$, or so-called magnetostatic modes. The spin wave theory is not strictly valid in describing these modes due to the negligence of the boundary conditions at the sample surfaces. Instability theories for magnetostatic modes in spheres have been developed by several authors [52,53,55-57]. A detail discussion of these theories is beyond the scope of this chapter.

7. Conclusion

This chapter has provided a tutorial review of the basic aspects of spin wave instability theory for ferrites. The emphasis was on the parametric excitation of spin waves under parallel pumping and perpendicular pumping configurations and the interpretation of these phenomena on the basis of first order nonlinear theory originally developed by Suhl and Schlömann. These phenomena are extremely important in the study of nonlinear dynamics in magnetic materials. The focus was specific to first order theory and the onset of instability. Steady state behavior in the nonlinear regime and the related effects such as auto-oscillations, chaos, and solitons are covered in later chapters.

Acknowledgements

The authors are indebted to many colleagues for helpful insights into the ideas and concepts presented here. Special recognition is due to Drs. J. J. Green, E. Schlömann, W. Jantz, and G. Wiese.

Appendix A. Magnetostatic Approximation

The so-called magnetostatic approximation is an approximation for the Maxwell equations in which electromagnetic propagation effects are ignored. This is one of the basic approximations implemented in the standard theories for spin waves and magnetostatic modes. Historically, the approximation bears the name "magnetostatic," though it is really for magnetic waves at microwave frequencies.

Consider the full set of Maxwell equations for the dynamic electric and magnetic fields, $\mathbf{e}(\mathbf{r},t)$ and $\mathbf{h}(\mathbf{r},t)$, and the dynamic magnetization $\mathbf{m}(\mathbf{r},t)$ for a magnetic insulator with a scalar dielectric constant ϵ.

$$\nabla\cdot\mathbf{e}(r,t) = 0 \ . \tag{A-1}$$

$$\nabla\times\mathbf{e}(\mathbf{r},t) = -\frac{1}{c}\frac{\partial}{\partial t}[\mathbf{h}(\mathbf{r},t) + 4\pi\mathbf{m}(\mathbf{r},t)] \ . \tag{A-2}$$

$$\nabla\cdot[\mathbf{h}(\mathbf{r},t) + 4\pi\mathbf{m}(\mathbf{r},t)] = 0 \ . \tag{A-3}$$

$$\nabla\times\mathbf{h}(\mathbf{r},t) = \frac{\epsilon}{c}\frac{\partial}{\partial t}\mathbf{e}(\mathbf{r},t) \ . \tag{A-4}$$

Here, c denotes the speed of light in free space. These equations are written in Gaussian units. The usual approach in the magnetostatic approximation is to write the $\nabla\times\mathbf{h}$ equation as

$$\nabla\times\mathbf{h}(\mathbf{r},t) = 0 \ , \tag{A-5}$$

thereby neglecting the time derivative driving term in Eq. (A-4). Equation (A-5), together with Eq. (A-3), leads to the well known spin wave dipole field expression developed in Sec. 2.

In this appendix, we consider spin wave components at wavenumber k and frequency ω_k for $\mathbf{h}(\mathbf{r},t)$ and $\mathbf{m}(\mathbf{r},t)$. We use the full Maxwell equations to obtain the connection between these components. We then establish the specific restrictions on k and ω_k for which the dipole field expression developed from Eq. (A-3) is valid. This defines the magnetostatic approximation.

From the full Maxwell equations, the wave equation for $\mathbf{h}(\mathbf{r},t)$ is

$$\nabla^2\mathbf{h}(\mathbf{r},t) - \frac{\epsilon}{c^2}\frac{\partial^2}{\partial t^2}\mathbf{h}(\mathbf{r},t)$$

$$= -4\pi\nabla[\nabla\cdot\mathbf{m}(\mathbf{r},t)] + 4\pi\frac{\epsilon}{c^2}\frac{\partial^2}{\partial t^2}\mathbf{m}(\mathbf{r},t) \ . \tag{A-6}$$

We now consider plane wave solutions for $\mathbf{h}(\mathbf{r},t)$ and $\mathbf{m}(\mathbf{r},t)$ with frequency ω_k and wave

vector **k**.

$$\mathbf{h}(\mathbf{r},t) = \mathbf{h}_k e^{i(\omega_k t - \mathbf{k}\cdot\mathbf{r})} . \tag{A-7a}$$

$$\mathbf{m}(\mathbf{r},t) = \mathbf{m}_k e^{i(\omega_k t - \mathbf{k}\cdot\mathbf{r})} . \tag{A-7b}$$

The relation between the time-independent amplitudes $\mathbf{h}_k$ and $\mathbf{m}_k$ obtained from Eq. (A-5) is given by

$$\mathbf{h}_k = -\frac{1}{k^2 - k_0^2} 4\pi \mathbf{k}(\mathbf{k}\cdot\mathbf{m}_k) + \frac{k_0^2}{k^2 - k_0^2} 4\pi \mathbf{m}_k . \tag{A-8}$$

Here, k_0 denotes the wavenumber for ordinary electromagnetic waves propagating with the same frequency ω_k in the medium.

$$k_0 = \frac{\omega_k}{c}\sqrt{\epsilon} . \tag{A-9}$$

For ferrites at 10 GHz and with a dielectric constant $\epsilon = 10$, the value of k_0 is 6.6 cm^{-1}.

The two terms in Eq. (A-8) have different physical origins. The $\mathbf{k}(\mathbf{k}\cdot\mathbf{m}_k)$ term derives from the microscopic magnetic dipole-dipole interaction, as discussed in Sec. 2.2. The $4\pi\mathbf{m}_k$ term derives from the time-derivative of the electric field and, therefore, may be called the electromagnetic propagation term. In a situation where the condition $|k| \gg k_0$ is satisfied, the contribution from the $4\pi\mathbf{m}_k$ term in Eq. (A-8) is negligible. In this limit, only the dipole field contribution remains and Eq. (A-8) can be approximated to

$$\mathbf{h}_k \approx -\frac{4\pi}{k^2} \mathbf{k}(\mathbf{k}\cdot\mathbf{m}_k) . \tag{A-10}$$

This form of the dipole field is utilized extensively in classical spin wave theory, as in Eq. (2-15). More discussions on electromagnetic propagation effects can be found in Smit and Wijn [58] and Auld [59].

It is important to note here that there is *no upper limit* on the range of k for this approximation. Many workers incorrectly made this limit part of the magnetostatic approximation by specifying that k be sufficiently small so that exchange fields may be neglected. The only limitation for the validity of Eq. (A-10), and hence the operational utility of Eq. (A-5), is the condition $|k| \gg k_0$.

Appendix B. Holstein-Primakoff Transformation

The linear equation of motion for spin waves in $\alpha_k(t)$ and $\alpha_{-k}^*(t)$ was obtained in Eq. (3-19) and given by

$$\frac{d}{dt}\begin{pmatrix} \alpha_k(t) \\ \\ \alpha_{-k}^*(t) \end{pmatrix} = i \begin{pmatrix} A_k & B_k \\ \\ -B_k^* & -A_k \end{pmatrix} \begin{pmatrix} \alpha_k(t) \\ \\ \alpha_{-k}^*(t) \end{pmatrix}, \tag{B-1}$$

with

$$A_k = \omega_H + |\gamma| D k^2 + \frac{1}{2}\omega_M \sin^2\theta_k , \tag{B-2a}$$

$$B_k = \frac{1}{2}\omega_M \sin^2\theta_k \, e^{i2\phi_k} . \tag{B-2b}$$

We seek a linear transformation of the form

$$\begin{pmatrix} b_k(t) \\ \\ b_{-k}^*(t) \end{pmatrix} = \begin{pmatrix} \lambda_k & \mu_k \\ \\ \mu_k^* & \lambda_k \end{pmatrix} \begin{pmatrix} \alpha_k(t) \\ \\ \alpha_{-k}^*(t) \end{pmatrix} \tag{B-3}$$

which will decouple the coupled $[\alpha_k(t), \alpha_{-k}^*(t)]$ modes. The formal approach for such a transformation starts with the basic eigenvalue equation for the matrix in Eq. (B-1).

$$\begin{vmatrix} A_k - \lambda & B_k \\ \\ -B_k^* & -A_k - \lambda \end{vmatrix} = 0 . \tag{B-4}$$

The two eigenvalues obtained from Eq. (B-4) are given by

$$\lambda_{1,2} = \pm\sqrt{A_k^2 - |B_k^2|} . \tag{B-5}$$

The transformation coefficients λ_k and μ_k in Eq. (B-3) are obtained in the usual manner for eigenvalue problems, based on the now determined eigenvalues $\lambda_{1,2}$ and the requirement that the transformed $[b_k(t), b_{-k}^*(t)]$ mode pair be uncoupled. One obtains the result of Holstein and Primakoff [23].

$$\lambda_k = \sqrt{(A_k + \omega_k)/(2\omega_k)} \ . \tag{B-6a}$$

$$\mu_k = \sqrt{(A_k - \omega_k)/(2\omega_k)}\, e^{i2\phi_k} \ . \tag{B-6b}$$

The $\lambda_{1,2}$ parameters correspond to the eigenfrequencies of our now uncoupled modes. We denote these eigenfrequencies as $\pm\omega_k$. The explicit form of ω_k from Eqs. (B-5) and (B-2) is given by

$$\omega_k = |\gamma| \sqrt{(H_{ext} - 4\pi M_s N_z + Dk^2)\,(H_{ext} - 4\pi M_s N_z + Dk^2 + 4\pi M_s \sin^2\theta_k)} \ . \tag{B-7}$$

This ω_k is the spin wave normal mode frequency in Eq. (3-26).

The spin wave equation of motion for $[b_k(t),\ b_{-k}^*(t)]$ is now written as

$$\frac{d}{dt}\begin{pmatrix} b_k(t) \\ \\ b_{-k}^*(t) \end{pmatrix} = i \begin{pmatrix} \omega_k & 0 \\ \\ 0 & -\omega_k \end{pmatrix} \begin{pmatrix} b_k(t) \\ \\ b_{-k}^*(t) \end{pmatrix} . \tag{B-8}$$

Equation (B-8) has simple uncoupled harmonic oscillator solutions for $b_k(t)$ and $b_{-k}^*(t)$.

$$b_k(t) = b_k e^{i\omega_k t} \ . \tag{B-9a}$$

$$b_{-k}^*(t) = b_{-k}^* e^{-i\omega_k t} \ . \tag{B-9b}$$

These are the classical spin wave normal modes. The overall transformation from the original $m_{kx}(t)$ and $m_{ky}(t)$ Fourier components of the dynamic magnetization to these spin wave normal modes is given by

$$\begin{pmatrix} b_k(t) \\ \\ b_{-k}^*(t) \end{pmatrix} = \frac{1}{M_s} \begin{pmatrix} \lambda_k + \mu_k & i(\lambda_k - \mu_k) \\ \\ \lambda_k + \mu_k^* & -i(\lambda_k - \mu_k^*) \end{pmatrix} \begin{pmatrix} m_{kx}(t) \\ \\ m_{ky}(t) \end{pmatrix} . \tag{B-10}$$

While the above procedure accomplishes the desired result in the form of explicit expressions for the spin wave dispersion and the normal mode transformation, the Holstein-Primakoff approach provides little physical insight into the nature of the spin wave modes. We conclude this appendix with an alternative derivation of the above transformation which provides such insight. This derivation is based on the work of Kemanis and Wang [25] and Helszajn [26,27].

It was noted in Sec. 2 that spin waves with $\mathbf{k} \cdot \mathbf{M}_s \neq 0$ are elliptically polarized, due to the fact that $\nabla \cdot \mathbf{m}(\mathbf{r},t)$ is nonzero. The elliptical precession cone for the spins is oriented with the major axis perpendicular to $\mathbf{k}$, the direction of propagation. Figure B-1

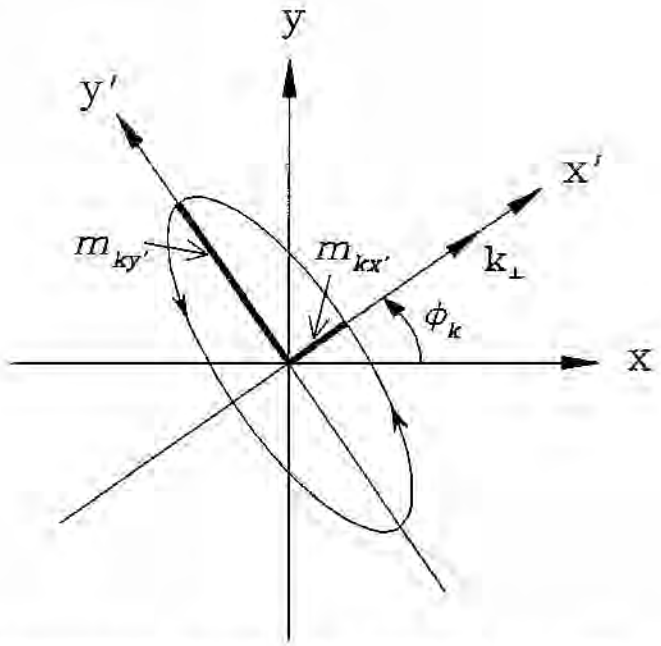

Figure B-1 Spin wave precessional cone projection in the x-y and x'-y' plane.

shows the x-y plane precession cone projection for a spin wave of wavevector $\mathbf{k}$ with some polar angle θ_k (not shown) and azimuthal angle ϕ_k. In the figure, the $\mathbf{k}_\perp$ vector is the projection of $\mathbf{k}$ on the x-y plane. This vector makes an angle ϕ_k with respect to the x-axis, consistent with Fig. 2-3. The new point here is the explicit realization of the elliptical precession geometry relative to our (x,y,z) reference frame. We have labeled the principal axes of the ellipse as x' and y'.

Now consider our starting equation of motion for $m_{kx}(t)$ and $m_{ky}(t)$ from Eq. (3-16).

$$\dot{m}_{kx}(t) = -\frac{1}{2}\omega_M \sin^2\theta_k \sin 2\phi_k \, m_{kx}(t) - (\omega_H + |\gamma| D k^2 + \omega_M \sin^2\theta_k \sin^2\phi_k) \, m_{ky}(t) \; . \tag{B-11a}$$

$$\dot{m}_{ky}(t) = (\omega_H + |\gamma| D k^2 + \omega_M \sin^2\theta_k \cos^2\phi_k) \, m_{kx}(t) + \frac{1}{2}\omega_M \sin^2\theta_k \sin 2\phi_k \, m_{ky}(t) \; . \tag{B-11b}$$

Based on Fig. B-1, we see that these x- and y-components of $\mathbf{m}_k(t)$ are not the simple 90° out-of-phase components evident from the elliptical precession picture. We now perform a coordinate rotation by a angle of ϕ_k, from (x,y) to (x',y'). The rotation serves to line up our new (x',y') axes with the axes of the elliptical precession cone projection in Fig.

B-1.

The dynamic magnetization components in the (x,y) and (x',y') coordinate systems are connected by the standard rotational transformation relations.

$$m_{kx'}(t) = \cos\phi_k\, m_{kx}(t) + \sin\phi_k\, m_{ky}(t) \ . \tag{B-12a}$$

$$m_{ky'}(t) = -\sin\phi_k\, m_{kx}(t) + \cos\phi_k\, m_{ky}(t) \ . \tag{B-12b}$$

In the new (x',y') coordinates, the transformed Eq. (B-11) is significantly simplified.

$$\dot{m}_{kx'}(t) = -(\omega_H + |\gamma| Dk^2)\, m_{ky'}(t) \ . \tag{B-13a}$$

$$\dot{m}_{ky'}(t) = (\omega_H + |\gamma| Dk^2 + \omega_M \sin^2\theta_k)\, m_{kx'}(t) \ . \tag{B-13b}$$

These two equations reflect the 90° out-of-phase condition for $m_{kx'}(t)$ and $m_{ky'}(t)$ magnetization components in the (x',y') frame. The general solutions for $m_{kx'}(t)$ and $m_{ky'}(t)$ are quite simple.

$$m_{kx'}(t) = m_{kx'} \cos(\omega_k t + \varphi_0) \ . \tag{B-14a}$$

$$m_{ky'}(t) = m_{ky'} \sin(\omega_k t + \varphi_0) \ . \tag{B-14b}$$

In the expressions above, φ_0 is an arbitrary initial phase and ω_k is the spin wave frequency discussed previously. We take the ratio $m_{kx'}/m_{ky'}$ as the ellipticity factor for the precession cone.

$$\frac{m_{kx'}}{m_{ky'}} = e_k \ . \tag{B-15}$$

This e_k-factor is obtained from Eq. (B-13) as

$$e_k = \sqrt{\frac{\omega_H + |\gamma| Dk^2}{\omega_H + |\gamma| Dk^2 + \omega_M \sin^2\theta_k}} = \frac{\omega_H + |\gamma| Dk^2}{\omega_k} \ . \tag{B-16}$$

It is clear from Eq. (B-16) that e_k is always equal to or less than 1. In the range of $0° \le \theta_k \le 90°$, the spin wave precession is circular and we have $e_k = 1$ when θ_k is 0°. The spin wave precession is elliptical and we have $e_k < 1$ when $0° < \theta_k \le 90°$ is satisfied.

We see that this simple rotational transformation yields both the spin wave frequency ω_k and additional physical insight into the nature of the elliptical spin wave precession modes in the classical theory. The $m_{kx'}(t)$ and $m_{ky'}(t)$ modes in Eq. (B-13) are still coupled, however. We decouple these modes to circularly polarized complex modes by a transformation in the same spirit of our previous transformation in Eq. (3-18) of Sec. 3. Here, however, we need to take the ellipticity of the precession into account in this

final transformation.

$$c_k(t) = \frac{1}{M_s}\left[m_{kx'}(t) + i e_k m_{ky'}(t)\right] , \tag{B-17a}$$

$$c^*_{-k}(t) = \frac{1}{M_s}\left[m_{kx'}(t) - i e_k m_{ky'}(t)\right] . \tag{B-17b}$$

The physical reason for including the ellipticity factor in the transformation is to compensate for the elongation of the spin wave precession component in the y'-axis and obtain a circularly polarized spin wave complex amplitude. Under the transformation of Eq. (B-17), the spin wave equation of motion becomes diagonal in the matrix form.

$$\frac{d}{dt}\begin{pmatrix} c_k(t) \\ \\ c^*_{-k}(t) \end{pmatrix} = i\begin{pmatrix} \omega_k & 0 \\ \\ 0 & -\omega_k \end{pmatrix}\begin{pmatrix} c_k(t) \\ \\ c^*_{-k}(t) \end{pmatrix} . \tag{B-18}$$

This equation is identical with the one obtained previously in Eq. (B-8). We now have realized the same basic result as from the Holstein-Primakoff approach, but the physics of the overall transformation is now clear. The normal spin wave modes are circularly polarized complex waves, with appropriate rotation and scaling to deal with the phases and ellipticity of the original spin precession components. The combined effect of the $(x,y)\rightarrow(x',y')$ rotational transformation and the $m_{kx'}(t)\pm ie_k m_{ky'}(t)$ complex circular transformation is obtained from Eqs. (B-12) and (B-17).

$$\begin{pmatrix} c_k(t) \\ \\ c^*_{-k}(t) \end{pmatrix} = \frac{1}{M_s}\begin{pmatrix} \cos\phi_k - ie_k\sin\phi_k & \sin\phi_k + ie_k\cos\phi_k \\ \\ \cos\phi_k + ie_k\sin\phi_k & \sin\phi_k - ie_k\cos\phi_k \end{pmatrix}\begin{pmatrix} m_{kx}(t) \\ \\ m^*_{ky}(t) \end{pmatrix} . \tag{B-19}$$

The connection between the above matrix and the Holstein-Primakoff transformation matrix of Eq. (B-10) is not obvious at first glance. In fact, these two matrices are similar. The top and bottom rows of the matrix above are related to the corresponding rows of the matrix in Eq. (B-10) by a scaling factor Q and its complex conjugate Q^*, respectively, with Q given by

$$Q = \frac{2\lambda_k}{1+e_k}\, e^{i\phi_k} . \tag{B-20}$$

These two transformations are, therefore, physically equivalent.

References

1. J. H. E. Griffiths, *Nature* **158** (1946) 670.
2. C. Kittel, *Phys. Rev.* **71** (1947) 270.
3. C. Kittel, *Phys. Rev.* **73** (1948) 155.
4. N. Bloembergen and R. W. Damon, *Phys. Rev.* **85** (1952) 699.
5. R. W. Damon, *Rev. Mod. Phys.* **25** (1953) 239.
6. N. Bloembergen and S. Wang, *Phys. Rev.* **93** (1954) 72.
7. R. W. Damon, in *Magnetism*, Vol. 1, ed. G. T. Rado and H. Suhl (Academic Press, New York, 1963).
8. H. Suhl, *J. Phys. Chem. Solids* **1** (1957) 209.
9. E. Schlömann, *Technical Report* **R-48**, Research Division, Raytheon Company, 1959 (unpublished).
10. F. Bloch, *Z. Physik* **61** (1930) 206.
11. C. Herring and C. Kittel, *Phys. Rev.* **81** (1951) 869.
12. L. Landau and E. Lifshitz, *Phys. Z. Sowjetunion* **8** (1935) 153.
13. C. E. Patton, *Phys. Rep.* **103** (1984) 251.
14. B. Lax and K. J. Button, *Microwave Ferrites and Ferrimagnetics* (McGraw-Hill, New York, 1962) p. 175.
15. V. E. Zakharov, V. S. L'vov, and S. S. Starobinets, *Usp. Fiz. Nauk* **114** (1974) 609 [*Sov. Phys. -Usp.* **17** (1975) 896].
16. G. Gibson and C. Jeffries, *Phys. Rev.* **A29** (1984) 811.
17. X. Y. Zhang and H. Suhl, *Phys. Rev.* **B38** (1988) 4893.
18. P. Bryant, C. Jeffries, and K. Nakamura, *Phys. Rev. Lett.* **60** (1988) 1185.
19. P. E. Wigen, R. D. McMichael, and C. Jayaprakash, *J. Magn. Magn. Mater.* 84 (1990) 237.
20. S. M. Rezende and F. M. de Aguiar, *Proc. IEEE* **78** (1990) 893.
21. G. Srinivasan, M. Chen, and C. E. Patton, *J. Appl. Phys.* **64** (1988) 5480.
22. C. E. Patton, *J. Appl. Phys.* **40** (1969) 2837.
23. T. Holstein and H. Primakoff, *Phys. Rev.* **58** (1940) 1098.
24. C. Kittel, *Quantum Theory of Solids* (Wiley, New York, 1987) p. 23.
25. G. Kemanis and S. Wang, *J. Appl. Phys.* **35** (1964) 1465.
26. J. Helszajn, *Proc. IEE* **114** (1967) 1585.
27. J. Helszajn, *Principles of Microwave Ferrite Engineering* (Wiley, London, 1969) p. 34.
28. A. M. Clogston, H. Suhl, L. R. Walker, and P. W. Anderson, *J. Phys. Chem. Solids* **1** (1956) 129.
29. J. J. Green, C. E. Patton, and E. Stern, *J. Appl. Phys.* **40** (1969) 172.
30. C. E. Patton, *J. Appl. Phys.* **41** (1970) 431.
31. Y. H. Liu and C. E. Patton, *J. Appl. Phys.* **53** (1982) 5116.
32. Yu. M. Yakovlev, Yu. M. Burdin, Yu. R. Shilnikov, and T. N. Bushueva, *Fiz. Tverd. Tela* **12** (1970) 3059 [*Sov. Phys. - Solid state* **12** (1971) 2475].
33. F. R. Morgenthaler, *J. Appl. Phys.* **31** (1960) 95 S.

34. F. R. Morgenthaler, Ph.D. Dissertation, MIT, 1960.
35. E. Schlömann, J. J. Green, and U. Milano, *J. Appl. Phys.* **31** (1960) 386 S.
36. E. Schlömann, *J. Phys. Soc. Jpn., Suppl. B-I*, **17** (1961) 406.
37. M. Sparks, R. Loudon, and C. Kittel, *Phys. Rev.* **122** (1961) 791.
38. M. Sparks, *Ferromagnetic Relaxation Theory* (McGraw-Hill, New York, 1964).
39. C. E. Patton, *Phys. Stat. Sol.* (b) **92** (1979) 211.
40. C. E. Patton, *Phys. Stat. Sol.* (b) **93** (1979) 63.
41. C. E. Patton and W. Jantz, *IEEE Trans. Mag.* **MAG-14** (1978) 698.
42. C. E. Patton and W. Jantz, *J. Appl. Phys.* **50** (1979) 7082.
43. J. C. Sethares, M. H. Seavey, T. G. Purnhagen, and M. R. Stiglitz, *J. Appl. Phys.* **35** (1964) 898.
44. C. E. Patton and J. J. Green, *IEEE Trans. Mag.* **MAG-4** (1969) 626.
45. W. Jantz and J. Schneider, *Solid State Commun.* **10** (1972) 937.
46. W. Jantz and J. Schneider, *Phys. Stat. Sol.* (a) **31** (1975) 595.
47. H. Suhl, *Phys. Rev.* **101** (1956) 1437.
48. R. C. LeCraw, E. G. Spencer, and C. S. Porter, *J. Appl. Phys.* **29** (1958) 326.
49. E. G. Spencer, R. C. LeCraw, and C. S. Porter, *J. Appl. Phys.* **29** (1958) 429.
50. F. C. Rossol, *J. Appl. Phys.* **31** (1960) 2273.
51. R. W. Cross, C. E. Patton, G. Srinivasan, J. G. Booth, and M. Chen, *J. Appl. Phys.* **69** (1991) 1569.
52. M. Chen and C. E. Patton, *J. Appl. Phys.* **69** (1991) 5724.
53. M. Chen, Ph. D. Dissertation, Colorado State University, 1991.
54. W. Jantz, W. Wettling, and J. Schneider, in *Physics of Magnetic Garnets*, ed. A. Paoletti (North-Hollan, Amsterdam, 1978).
55. P. H. Bryant, *Phys. Rev.* **B39** (1989) 4363.
56. G. Wiese and H. Benner, *Z. Phys.* **B79** (1990) 119.
57. G. Wiese, *Z. Phys.* **B82** (1991) 453.
58. J. Smit and H. P. J. Wijn, *Ferrites* (Wiley, New York, 1959) p. 92.
59. B. A. Auld, *J. Appl. Phys.* 31 (1960) 1642.